Evolution of ore-forming fluids in a post-collisional porphyry Cu-Au system: A case study from the Bučim deposit, Republic of North Macedonia

Strmić Palinkaš, Sabina; Perković, Ivor; Čobić, Andrea; Jurković, Iva; Tasev, Goran; Serafimovski, Todor; Spangenberg, Jorge E.

Ore Geology Reviews 146 (2022) 104913

Contents lists available at ScienceDirect

Ore Geology Reviews

journal homepage: www.elsevier.com/locate/oregeorev

Evolution of ore-forming fluids in a post-collisional porphyry Cu-Au system: A case study from the Bučim deposit, Republic of North Macedonia

Sabina Strmić Palinkaš [a,b,*], Ivor Perković [c], Andrea Čobić [d], Iva Jurković [d,e], Goran Tasev [f], Todor Serafimovski [f], Jorge E. Spangenberg [g]

[a] UiT The Arctic University of Norway, Faculty of Sciences and Technology, Department of Geosciences, Dramsvegen 201, N-9037 Tromsø, Norway
[b] University of Bergen, Faculty of Mathematics and Natural Sciences, Department of Earth Science, Centre for Deep Sea Research, Allegaten 41, N-5007 Bergen, Norway
[c] University of Zagreb, Faculty of Mining, Geology, and Petroleum Engineering, Pierottijeva 6, HR-10000 Zagreb, Croatia
[d] University of Zagreb, Faculty of Science, Department of Geology, Horvatovac 95, HR-10000 Zagreb, Croatia
[e] Prehnit Ltd., Garićka 11, HR-10000 Zagreb, Croatia
[f] Goce Delčev University, Faculty of Natural and Technical Sciences, Goce Delčev 89, MK-2000 Štip, North Macedonia
[g] University of Lausanne, Institute of Earth Surface Dynamics, Geopolis, CH-1015 Lausanne, Switzerland

A B S T R A C T

The Bučim porphyry Cu-Au deposit is situated in the westernmost part of the Serbo-Macedonian Massif, Republic of North Macedonia. The deposit is hosted by Precambrian gneisses with tectonically imbedded rare lenses of Palaeozoic amphibolites. The mineralization is spatially associated with intrusions of andesitic to trachyandesitic magmatic bodies. The geochemical signature of the intrusions and their radiogenic age suggest that the Bučim porphyry Cu-Au deposit represents a product of the Oligocene/Early Miocene post-collisional magmatic activity. The Vršnik intrusion, the youngest among four intrusions at the Bučim deposit, has not been subjected to later magmatic overprints and was therefore selected for studying the evolution of ore-forming fluids in post-collisional porphyry Cu-Au systems.

The Cu-Au mineralization is spatially associated with hydrothermal alteration assemblages within and around the Vršnik intrusion. The infiltration of hot, near-neutral, oxidized, and highly saline and metal-rich aqueous solutions developed a mineralized potassic alteration zone. The fluid inclusion study suggests the formation temperature and pressure of 600-645°C and 0.675 kbar, respectively. This alteration zone is characterized by the replacement of amphibole with biotite and crystallization of hydrothermal biotite, magnetite, and hematite within the fine-grained groundmass of the intrusion. The oxidation of ferrous to ferric iron in this alteration zone has been recognized as a possible trigger for sulfate reduction and the consequent deposition of sulfide mineralization.

The fluid inclusion study reflects that the barren phyllic alteration zone represents a product of infiltration of hot and saline fluids with a high metal-transport capability. Anyhow, sericitization and silicification suggest a low pH that might have played a significant role in preventing Cu deposition. The stable isotope composition of carbonates associated with the phyllic alteration zone point to a contribution of magmatic CO_2.

The mineralized chlorite alteration zone is mainly well developed along the contact between the intrusion and surrounding gneisses and reflects conditions of a high water/rock ratio. The fluid inclusion assemblages composed exclusively of vapor-rich inclusions indicate fluid flashing, probably associated with the transition from the lithostatic to hydrostatic regime at the point when the system cooled down to approximately 400°C. The liquid + vapor fluid inclusion assemblages point to dilution and cooling episodes, apparently related to mixing of ore-bearing fluids and meteoric water. The decrease in temperature as well as the decrease in the fluid salinity are associated with the mobility of metals transported in forms of their chloride complexes, including Cu, Au and Ag.

The barren argillic alteration zone was developed under the influence of relatively cold and diluted fluids, with very limited capability for transport of metals. The water/rock ratio was relatively high but lower comparing the chlorite alteration zone.

The presented study revealed that development of hydrothermal alteration zones and evolution of ore-forming fluids in post-collisional porphyry Cu-Au systems are comparable with those known from subduction-related magmatic arcs.

1. Introduction

Porphyry Cu-Au deposits are well known as the world's most important source of Cu and an important source of Au (e.g., Richards, 2003; Sillitoe, 2010; Park et al., 2019), but recently they have also started to attract attention as a potential source of numerous technology critical elements (Stergiou et al., 2021). These deposits usually range in size from 10 Mt to several billion tonnes, and their average Cu grade is often < 0.5 wt% (Sinclair, 2007). Numerous well studied giant porphyry Cu deposits (e.g., Escondida, Chile; Toquepala, Peru; Bingham Canyon, USA; Grasberg, Indonesia) have been genetically associated with subduction-related magmatic arcs (e.g., Richards et al., 2001; Richards,

* Corresponding author.
E-mail address: sabina.s.palinkas@uit.no (S. Strmić Palinkaš).

https://doi.org/10.1016/j.oregeorev.2022.104913
Received 11 January 2022; Received in revised form 21 April 2022; Accepted 21 April 2022
Available online 27 April 2022

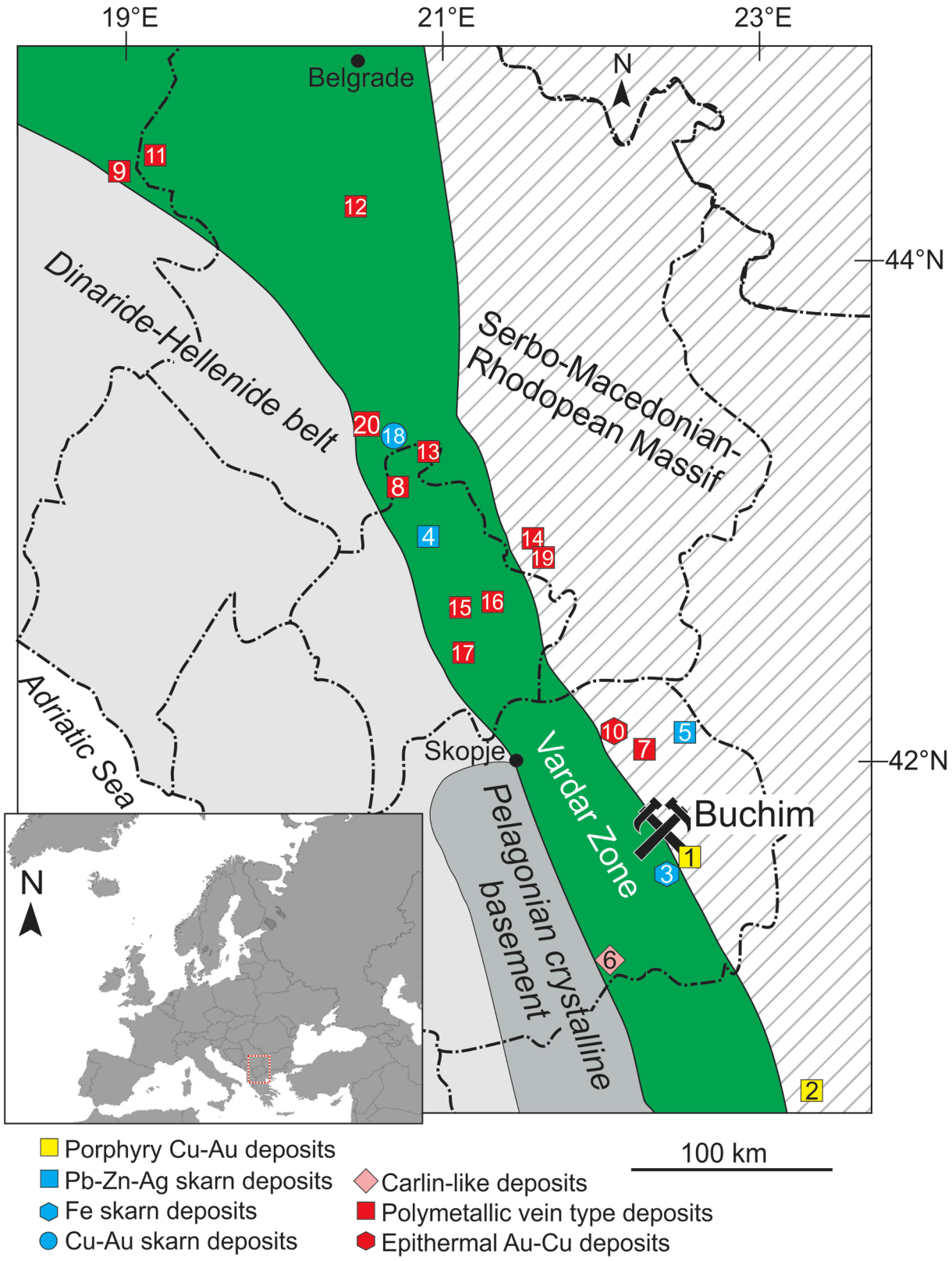

Fig. 1. Regional geologic setting of the Bučim porphyry Cu-Au deposit, North Macedonia, within the Balkan Peninsula (modified after Dimitrijevic (2001) and Karamata (2006)). The locations of the most prominent Tertiary magmatic-hydrothermal and hydrothermal deposits are also marked: 1-Borov Dol; 2- Skouries; 3-Damjan; 4-Trepča; 5-Sasa; 6-Allchar; 7-Zletovo; 8-Crnac; 9- Čumavići; 10-Plavica; 11-Boranja; 12-Rudnik; 13-Belo Brdo; 14-Leče; 15-Badovac 16-Avajllija; 17-Kišnica; 18- Karavansalija; 19-Tulare; 20-Raška.

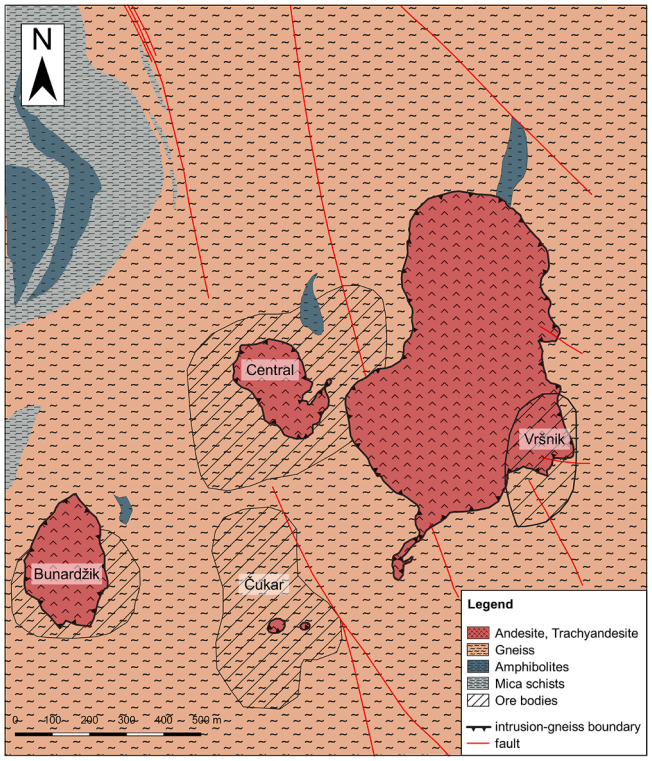

Fig. 2. Geological map of the Bučim porphyry Cu-Au deposit (modified after Serafimovski and Boev, 1996).

2003; Sillitoe, 2010). However, recently it has been suggested that post-subduction magmatism, associated with either lithospheric thickening during collision or decompression melting during post-collisional extension, may also result with formation of porphyry Cu mineralization (Richards, 2009; Müller and Groves, 2016; Wang et al., 2018; Delibaş et al., 2019).

Numerous Oligocene to Pliocene mineral deposits located along the Balkan Peninsula in SE Europe record evidence of a tight time–space relationship between post-collisional magmatism and magmatic-hydrothermal and hydrothermal ore-forming processes (Fig. 1; Cvetković et al., 2004; Yanev et al., 2008, Lehmann et al., 2013). The magmatic-hydrothermal mineral deposits are mostly represented by porphyry Cu-Au mineralization (e.g., Skouries deposit, Greece, Kroll et al., 2002; Bučim and Borov Dol deposits, North Macedonia, Serafimovski et al., 2010) and skarn mineralization (e.g., Damjan Fe skarn deposit, North Macedonia, Lehmann et al., 2013; Trepča Pb-Zn-Ag skarn deposit, Kosovo, Strmić Palinkaš et al., 2013; Sasa Pb-Zn-Ag skarn deposit, North Macedonia, Strmić Palinkaš et al., 2018a; Karavansalija Cu-Au skarn deposit, Serbia, Hoerler et al., 2022). The hydrothermal deposits range from deep-seated Carlin-like mineralization (e.g., Allchar deposit, North Macedonia, Strmić Palinkaš et al., 2018b), polymetallic vein mineralization (e.g., Zletovo Pb-Zn deposit, North Macedonia, Tasev and Serafimovski, 2012; Crnac Pb-Zn-Ag deposit, Kosovo, Borojević Šoštarić et al., 2012; Čumavići Sb-Zn-Pb-Ag deposit, Bosnia and Herzegovina, Radosavljević et al., 2016; Tulare Pb-Zn deposit, Velojić et al., 2018) up to epithermal mineralization (e.g., Plavica Au-Cu deposit, North Macedonia, Melfos et al., 2019).

The primary goal of the study was to assess the physicochemical conditions that control evolution of ore-forming fluids during formation of post-collisional porphyry Cu-Au deposits. Here we present the results of a case study, including mineral and chemical composition of hydrothermal alterations, mineral composition of ore-bearing parageneses as well as fluid inclusion and stable isotope data obtained from the Vršnik ore body of the Bučim deposit, North Macedonia (Fig. 1). With total mineral reserves of 170 Mt and historical production close to 150 Mt at

Fig. 3. Satellite image of the Vršnik open pit, the Bučim porphyry Cu-Au deposit, North Macedonia, with marked sampling locations (source: Google Maps, 2020).

0.3 wt% Cu and 0.3–0.5 g/t Au (Serafimovski et al., 2016), the Bučim deposit is one of the smallest mined porphyry Cu-Au deposits in the world. Still, despite its small size, the deposit contains well-preserved records of the evolution of Cu-Au-ore-forming fluids in post-collisional settings, particularly in the youngest Vršnik ore body.

2. Geological setting

2.1. Regional geology

The Vardar Zone, the main suture zone between the Adriatic plate, to the west, and the Eurasian plate, to the east, occupies the central part of the Balkan Peninsula (Fig. 1). The formation of this tectonostratigraphic unit started with the intracontinental rifting in the Late Permian to Middle Triassic that was followed by the opening of the Tethyan Ocean and deposition of the subsiding carbonate platform during the Late Triassic to Early Jurassic time (Sharp and Robertson, 2006; Dilek et al., 2007; Robertson et al., 2013). Closure of the Tethyan Ocean in the Middle Jurassic to Early Cretaceous (Borojević Šoštarić et al., 2014) was succeeded by the Upper Cretaceous subduction and collision that started at the beginning of the Tertiary (Cvetković et al., 2004; Márton et al., 2022).

To the east, the Vardar Zone is bordered by the Serbo-Macedonian Massif (Fig. 1; Dimitrijević, 2001; Karamata, 2006; Robertson et al., 2013), a Precambrian to Palaeozoic terrain, composed of two main tectonostratigraphic units. The Lower Unit of the Serbo-Macedonian Massif (also known as the Lower Complex in Serbia and North Macedonia, the Ograzhden Unit in Bulgaria and the Vertiskos Unit in

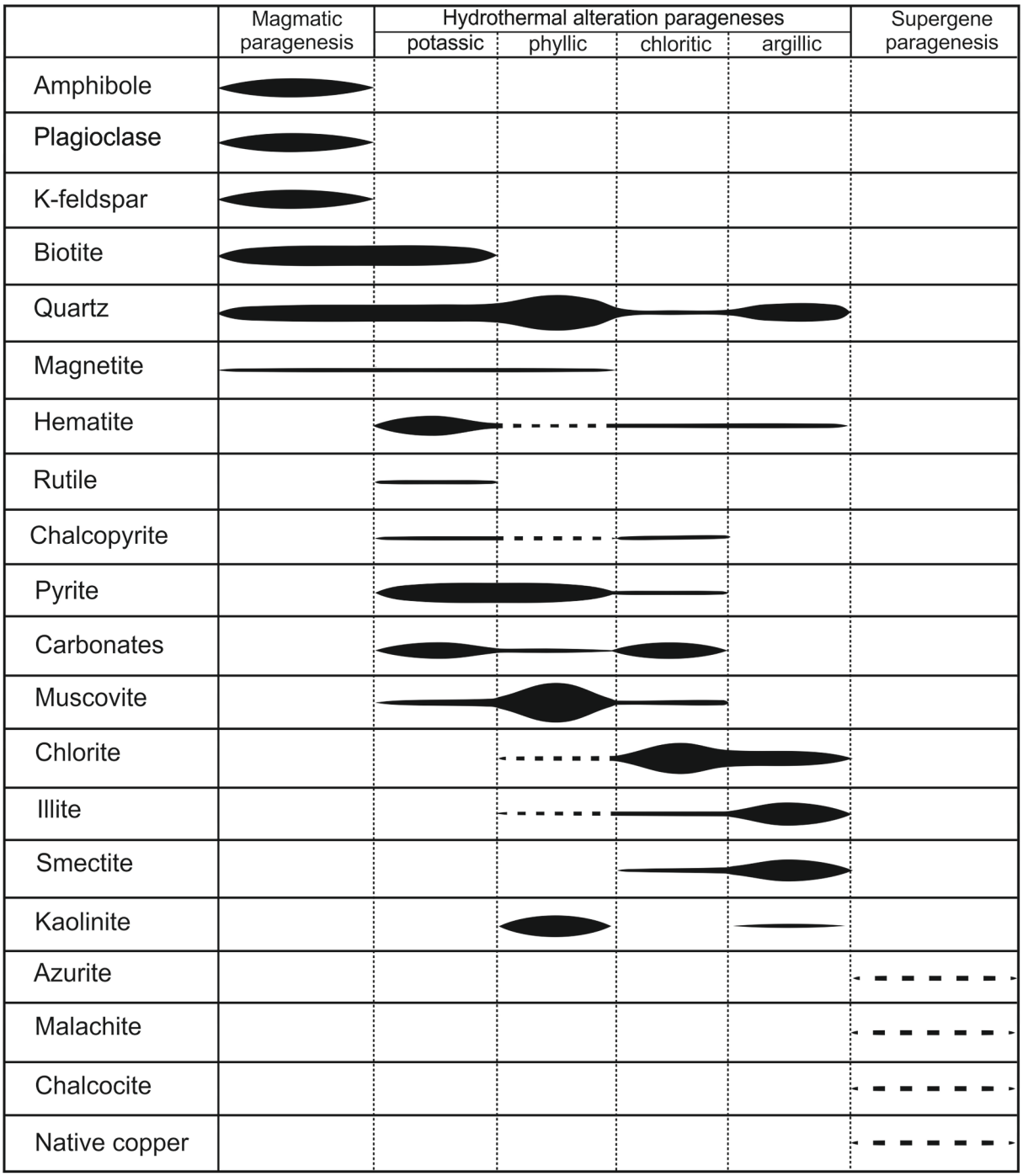

Fig. 4. Paragenetic sequence of the Vršnik ore body, the Bučim porphyry Cu-Au deposit, North Macedonia.

Greece) is a metamorphosed volcano-sedimentary sequence formed in the late Neoproterozoic to the earliest Cambrian along the active margin of north Gondwana. It is predominately composed of gneisses, micaschists, quartzites, amphibolites, and occasionally marbles and migmatites. The Lower Unit was metamorphosed up to medium- to lower-amphibolite facies during the Variscan orogeny (Dimitrijević, 2001; Antić et al., 2016a; Antić et al., 2016b). The Upper unit (the Vlasina Unit in Serbia and North Macedonia or the Morava Unit in Bulgaria) consists of the late Neoproterozoic ocean floor sediments and igneous rocks, overlain by a Lower Ordovician to Lower Carboniferous sedimentary sequence metamorphosed to greenschist facies (Zagorčev and Bončeva, 1988; Dimitrijević, 2001; Vasković, 2002).

In the Oligocene to Pliocene period (29.0 to 1.8 Ma), the Serbo-Macedonian massif and the Vardar Zone were affected by post-collisional collapse of the Alpine orogen, followed by extension and extensive magmatism of an intermediate, mostly andesitic to trachytic, character (Cvetković et al., 2004; Prelević et al., 2005; Melfos and Voudouris, 2017; Molnár et al., 2021).

2.2. Geology of the Bučim porphyry Cu-Au deposit

The Bučim deposit, a small Au-rich porphyry Cu deposit, is situated in the westernmost part of the Serbo-Macedonian Massif, along its contact with the Vardar Zone (Serafimovski et al., 2016; Fig. 1). The deposit is hosted by Precambrian gneisses intercalated with rare lenses of Palaeozoic amphibolites (Fig. 2). The mineralization is spatially

associated with andesite and trachyandesite intrusions of $^{206}Pb/^{238}U$ age between 24.04 ± 0.77 and 24.51 ± 0.89 Ma (Lehmann et al., 2013).

The Bučim deposit consists of four ore bodies (Central, Vršnik, Bunardžik and Čukar, Fig. 2). The Čukar ore body is composed of a supergene mineralization (Čifliganec, 1993), while the mineralization of the Central and Bunardžik ore bodies is of hypogene character and mostly consists of sulfide veinlets hosted by Precambrian gneisses along their contacts with porphyry intrusions. The Vršnik ore body is associated with the youngest intrusion in the Bučim deposit. The mineralization occurs in the intrusion as well as in the surrounding Precambrian gneisses (Fig. 2). The hypogene mineralization consists of sulfide disseminations and veinlets (Čifliganec, 1993; Lehmann et al., 2013). The main ore mineral is chalcopyrite accompanied by variable amounts of pyrite, magnetite, hematite, cubanite, valerite and bornite (Serafimovski and Boev, 1996). The supergene mineralization composed of azurite, malachite, chalcocite and minor amounts of native copper locally overprints the primary ore body (Serafimovski et al. 2016).

2.3. Samples and methods

A total of 20 samples was collected from the Vršnik ore body (Fig. 3). A relatively fresh sample of the magmatic intrusion was also included.

Paragenetic relationships were studied in thin polished sections by transmitted and reflected polarized light microscopy. The X-ray powder diffraction (XRD) was conducted on the bulk samples collected from the defined hydrothermal alteration zones at the Vršnik ore body. The analyses were performed at the University of Zagreb using a Philips PW 3040/60 X'Pert PRO powder diffractometer (45 kV, 40 μA), with CuKα-monochromatized radiation (λ = 1.54056 Å) and θ–θ geometry. The area between 4° and 63° 2θ, with 0.02° steps, was measured with a 0.5° primary beam divergence. The phase identification was performed in X' Pert high score Plus ver 2.0. In addition, oriented samples of the < 2 μm fraction from selected samples were prepared for clay mineral identification on air-dried, ethylene–glycol saturated, and heated (at 400 and 550 °C, respectively) samples, according to the procedure described by Starkey et al. (1984). Instrumental conditions were 40 kV, 40 mA, and constant time 5 s, with step scanning (0.02°2θ).

Lithogeochemical analyses of the fresh and altered host rocks were carried out at Bureau Veritas Commodities Canada using the LF200 method. Approximately 5 g of sample powder was mixed with lithium metaborate/tetraborate and fused to ensure total acid dissolution of refractory minerals such as xenotime, monazite, and zircon prior to analysis to determine major and trace element contents. Details on accuracy and precision can be found at http//https://www.acmelab.com.

The textural features and semi-quantitative analyses of mineralized samples were examined by a Zeiss Merlin Compact VP field emission Scanning Electron Microscope (SEM) equipped with an Energy-Dispersive X-ray (EDX) spectrometer at UiT The Arctic University of Norway. EDX analyses were conducted with an X-Max80 EDX detector by Oxford instruments at a working distance of 8.5 mm, using an accelerating voltage of 20 kV and an aperture of 60 μm. The samples were mechanically polished and carbon-coated. The retrieved data were further processed by applying the AZtec software provided by Oxford instruments.

Petrographic and microthermometric analyses of fluid inclusions within transparent quartz associated with the ore mineralization were performed at UiT The Arctic University of Norway. Double polished, 0.1 mm to 0.3 mm thick, transparent mineral wafers were studied. For the temperature range between −180 and +600 °C, measurements were carried out on a Linkam THMS 600 stage while higher homogenization temperatures were recorded using a Linkam TS1400XY stage. Both stages were mounted on an Olympus BX 2 using 10 × and 50 × Olympus long-working distance objectives. Two synthetic fluid inclusion standards (SYN FLINC; pure H_2O and mixed H_2O–CO_2) were used to calibrate the equipment. The precision of the system was ±2.0 °C for homogenization temperatures and ±0.2 °C in the temperature range

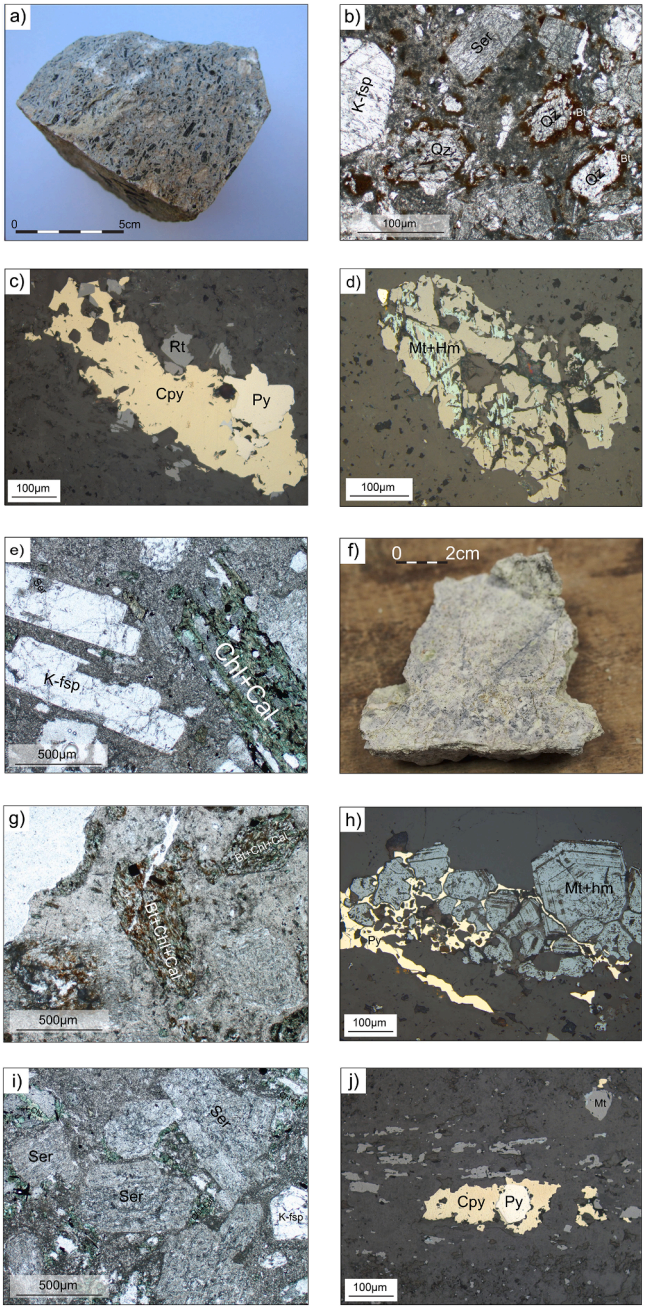

Fig. 5. .a) A hand specimen of the fresh portion of the Vršnik intrusion; **b)** Photomicrograph of the Vršnik intrusion altered to a potassic alteration assemblage (transmitted plane-polarized light); **c)** Photomicrograph of the disseminated sulfide mineralization associated with the potassic alteration zone (reflected plane-polarized light); **d)** Photomicrograph of the disseminated Fe-oxides associated with the potassic alteration zone (reflected plane-polarized light); **e)** Photomicrograph of the Vršnik intrusion altered to a phyllic alteration assemblage (transmitted plane-polarized light); **f)** A hand specimen of the Vršnik intrusion altered to a phyllic alteration assemblage showing an intensive alteration of the rock matrix but partly preserved porphyritic texture; **g)** Photomicrograph of the Vršnik intrusion altered to an argillic alteration assemblage (transmitted plane-polarized light); **h)** Photomicrograph of the ore mineralization associated with the argillic alteration zone (reflected plane-polarized light); **i)** Photomicrograph of the Vršnik intrusion altered to a chlorite alteration assemblage (transmitted plane-polarized light); **j)** Photomicrograph of the ore mineralization associated with the chlorite alteration zone (reflected plane-polarized light).

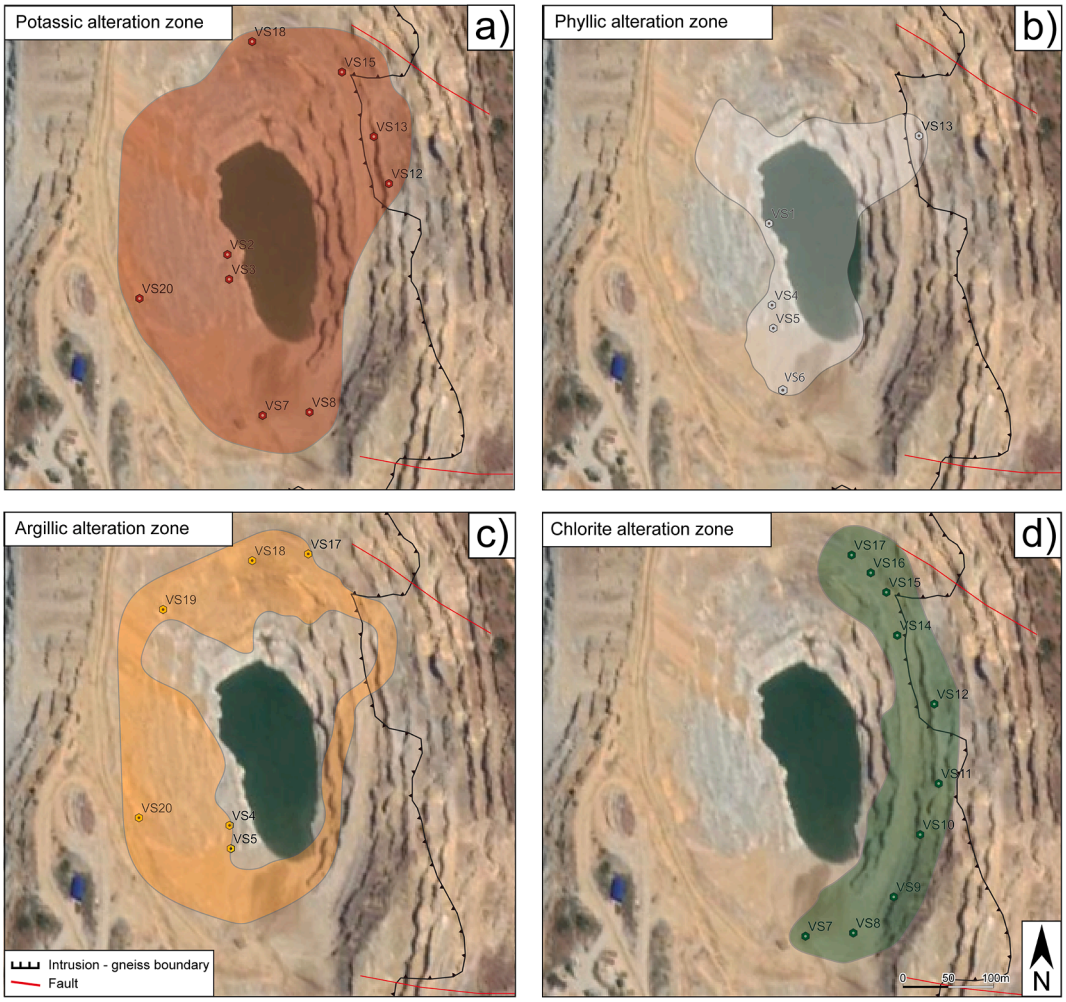

Fig. 6. Horizontal distribution of the alteration zones associated with the Vršnik ore body, the Bučim porphyry Cu-Au deposit, North Macedonia.

between −60° and +10 °C. Microthermometric measurements were conducted on defined fluid inclusion assemblages (FIAs), representing groups of inclusions that were trapped simultaneously. The FIAs were identified based on petrographic analysis before heating and freezing (Goldstein, 2001; Bodnar, 2003). During microthermometric measurements, the following phase transitions were recorded: the first-melting temperature (eutectic T_e), the last melting temperature of hydrohalite ($T_{m\ hh}$), last melting temperature of ice ($T_{m\ ice}$), last melting temperature of halite (T_s), and the total homogenization temperature (T_H). Calculations of compositions, densities, and isochores were conducted applying the numerical model by Steele-MacInnis et al. (2011) for the H_2O-NaCl-$CaCl_2$ system and Steele-MacInnis et al. (2012) for the H_2O-NaCl system.

Carbon and oxygen isotope analyses of calcite and siderite separated from the ore-bearing mineral assemblages were performed at the University of Lausanne, using a Thermo Fisher Scientific (Bremen, Germany) carbonate preparation device and Gas Bench II connected to a Delta Plus XL isotope ratio mass spectrometer (Révész and Landwehr 2002). Carbonate powder was extracted from hand-picked samples using a dental drill. The CO_2 extraction was performed by reaction of a 200–250 μg sample with 100% phosphoric acid at 70 °C for calcite and 90 °C for siderite. The isotope ratios are reported in the delta (δ) notation as the per mil (‰) deviation relative to the Vienna Peedee belemnite standard (VPDB). The normalization of the measured δ values to the VPDB scale was done with within-run replicate measurements of the laboratory standard Carrara marble ($\delta^{13}C = +2.05‰$, $\delta^{18}O = -1.7‰$), calibrated with international reference materials NBS 18 (carbonatite, $\delta^{13}C = -5.04‰$, $\delta^{18}O = -23.00‰$) and NBS 19 (limestone, $\delta^{13}C = +1.95‰$, $\delta^{18}O = -2.19‰$). The $\delta^{18}O$ values of siderite samples were corrected for the temperature dependence of the kinetic oxygen isotope fractionation between phosphoric acid liberated CO_2 and carbonate using the oxygen isotope fractionation equations of Das Sharma et al. (2002) and Rosenbaum and Sheppard (1986). All the $\delta^{18}O$ values were expressed relative to VSMOW (Vienna Standard Mean Ocean Water). Analytical uncertainty (1σ) monitored by replicate analyses of the laboratory standard Carrara marble was not greater than ±0.05‰ for $\delta^{13}C$ and ±0.1‰ for $\delta^{18}O$.

3. Results

3.1. Petrographic characteristics of the Vršnik ore body

The paragenetic sequence of the Vršnik ore body (Fig. 4) illustrates that ore deposition was associated with extensive hydrothermal alteration of the host intrusion, similar to other porphyry Cu deposits worldwide (e.g., Cooke et al., 2005; Sillitoe, 2010; Cooke et al., 2014). Relatively fresh parts of the Vršnik intrusion are characterized by a porphyritic texture with very fine-grained groundmass. Plagioclase, K feldspar, and amphibole are the most abundant phenocrysts. They occur as up to 1 cm long and 0.5 mm wide euhedral to subhedral crystals (Fig. 5a).

The potassic alteration zone (Fig. 6a; Fig. 7) preserves the original porphyritic texture (Fig. 5b). This alteration zone is characterized by extensive replacement of amphibole with biotite and crystallization of hydrothermal biotite within the fine-grained groundmass (Fig. 5c).

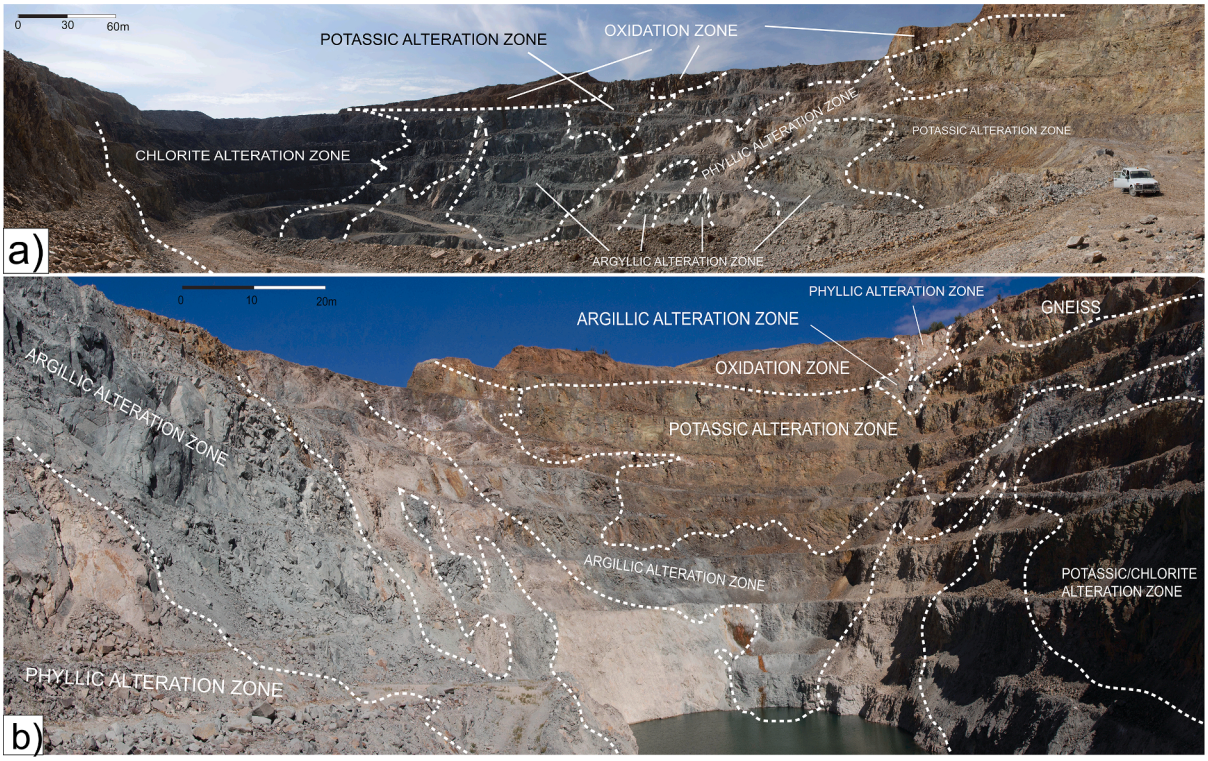

Fig. 7. Vertical distribution of the alteration zones within the Vršnik ore body, the Bučim porphyry Cu-Au deposit, North Macedonia.

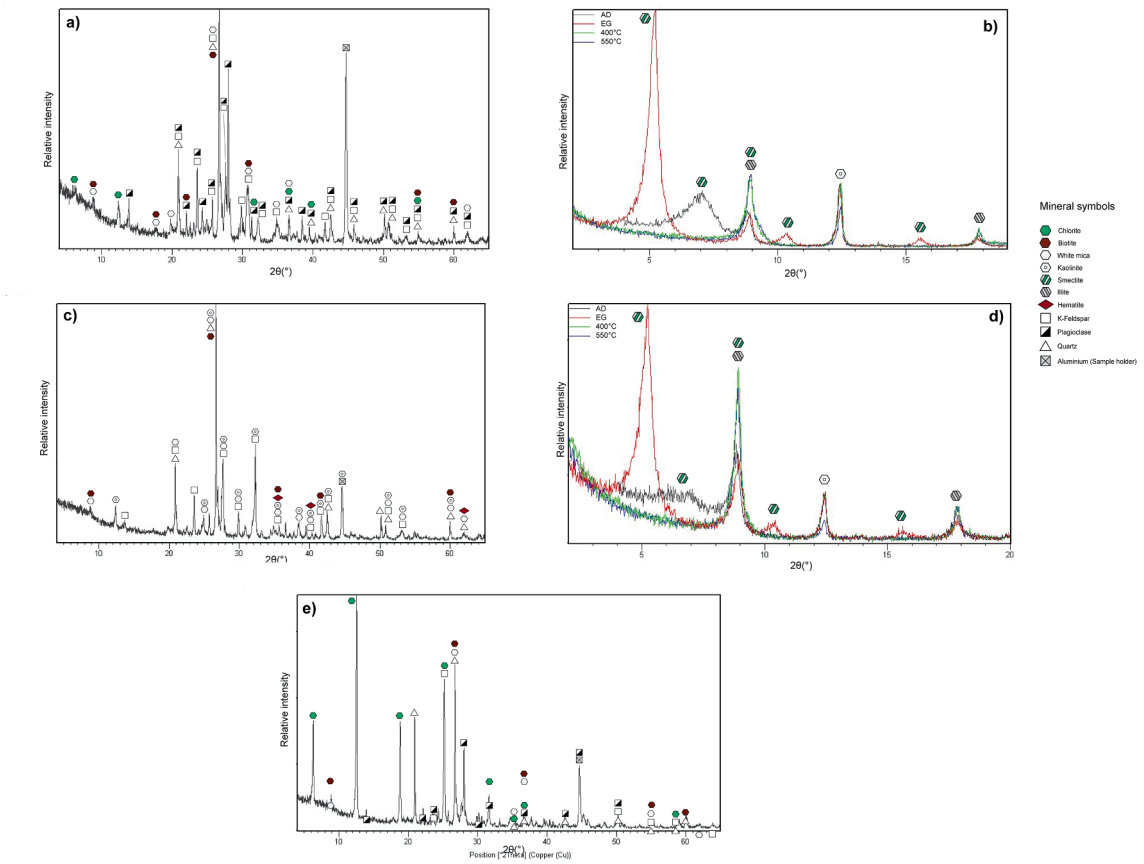

Fig. 8. Typical XRD patterns for **a)** a potassic alteration assemblage overprinted by phyllic and argillic alterations; **b)** a potassic alteration assemblage overprinted by chlorite alteration; **c)** a phyllic alteration assemblage; **d)** an argillic alteration assemblage; **e)** a chlorite alteration assemblage associated with the Vršnik ore body, the Bučim porphyry Cu-Au deposit, North Macedonia.

Table 1
Major element compositions of the fresh and altered parts of the Vrshnik intrusion, the Buchim porphyry Cu-Au deposit, North Macedonia.

Sample	Sample type	SiO_2	Al_2O_3	Fe_2O_3	MgO	CaO	Na_2O	K_2O	TiO_2	P_2O_5	MnO	Cr_2O_3	LOI	Sum
							wt.%							
	MDL	0.01	0.01	0.04	0.01	0.01	0.01	0.01	0.01	0.01	0.01	0.002	−5.1	0.01
VS1	Phyllic alteration	59.00	15.22	5.55	1.76	2.44	3.09	5.76	0.52	0.34	0.10	<0,002	5.9	99.76
VS6	Argillic alteration	59.75	15.44	6.49	2.75	1.93	2.64	5.50	0.50	0.28	0.21	<0,002	4.2	99.82
VS8	Potassic alteration	65.48	12.65	8.01	0.87	0.51	0.98	6.52	0.39	0.24	0.04	<0,002	3.9	99.70
VS9	Chlorite alteration	60.37	16.07	6.14	1.75	0.60	1.83	8.98	0.50	0.38	0.05	<0,002	2.1	98.89
VSR	Fresh rock	60.65	16.53	5.72	1.87	3.56	3.94	4.29	0.53	0.32	0.07	<0,002	1.9	99.61

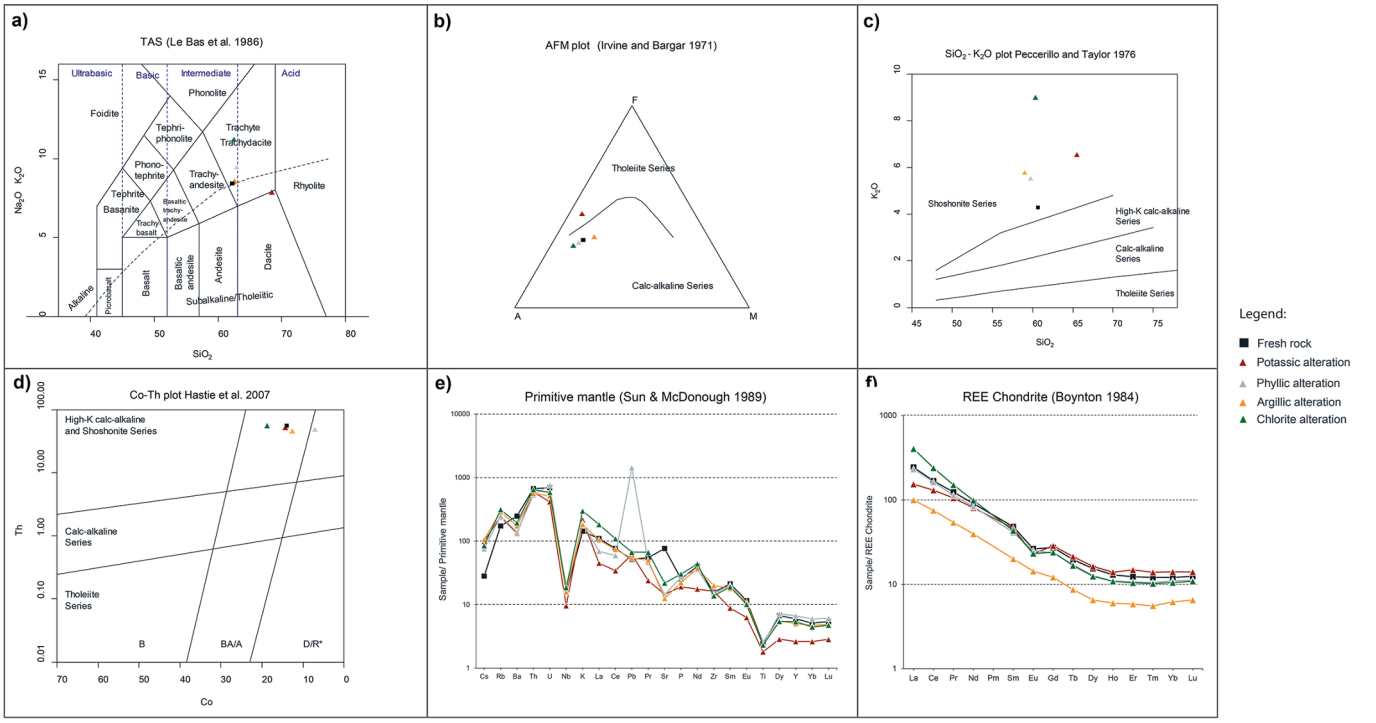

Fig. 9. Lithogeochemical data obtained from the fresh and altered portions of the Vršnik intrusion. **a)** Total Alkali vs Silica diagram (after Le Bas et al., 1986); **b)** AFM diagram (after Irvine and Baragar, 1971); **c)** K_2O vs SiO_2 diagram (after Peccerillo and Taylor, 1976); **d)** Co vs Th diagram (after Hastie et al., 2007); **e)** spider plots (after Boynton, 1984); **f)** chondrite normalized plots of REE concentrations (after Boynton, 1984).

Plagioclase is partly sericitized (Fig. 5c). The ore mineralization mainly occurs as disseminated pyrite and chalcopyrite, associated with variable amounts of rutile (Fig. 5d). Disseminated grains of magnetite and hematite are also common (Fig. 5e). Quartz veinlets with pyrite occur sporadically.

The phyllic alteration zone (Fig. 6b; Fig. 7) partly preserves the original porphyritic texture (Fig. 5e). Plagioclase is completely altered to a mixture of sericite and kaolinite. In contrast, K-feldspar is usually well preserved. Amphibole is mainly replaced by a mixture of chlorite and carbonates or locally by quartz. The groundmass is strongly altered to a mixture of sericite, kaolinite, and smectite (Fig. 5f). In contrast to the potassic alteration zone, the phyllic alteration zone is mostly barren.

The argillic alteration zone (Fig. 6c; Fig. 7) sporadically preserves the original porphyritic texture (Fig. 5g). Plagioclase and K-feldspar have been altered to a mixture of greenish clay minerals, probably smectite and illite. Previously biotitized amphiboles have been partly overprinted by a mixture of calcite and chlorite. The ore mineralization consists of disseminated pyrite, magnetite, and hematite (Fig. 5h). Veinlets, composed of quartz, calcite, siderite and minor amounts of pyrite, are also associated with this alteration zone.

The original porphyritic texture has mostly been disturbed (Fig. 5i) in the chlorite alteration zone (Fig. 6d; Fig. 7). This zone is characterized by the alteration of magmatic mafic minerals to chlorite. The mineralization mostly occurs as disseminated pyrite and chalcopyrite associated with variable amounts of magnetite (Fig. 5k). Quartz-carbonate veinlets with pyrite and chalcopyrite occur sporadically.

3.2. X-ray diffraction (XRD) of the hydrothermal alteration zones

The XRD analyses of the representative samples collected from the defined alteration zones (Fig. 6; Fig. 7) revealed that the potassic alteration was overprinted to various degrees by phyllic, argillic, and/or chlorite alterations (Fig. 8a; Fig. 8b). The XRD patterns obtained from samples collected in the phyllic alteration zone confirm the complete hydrothermal degradation of plagioclases, while K-felspars are, at least partly, preserved in this zone (Fig. 8c). The argillic alteration is characterized by abundant smectite, kaolinite, and illite (Fig. 8d). A typical alteration assemblage from the chlorite alteration zone predominantly consists of chlorite, quartz, and muscovite (Fig. 8e).

3.3. Lithogeochemistry of the Vršnik intrusion

The major element compositions of the fresh portion of the Vršnik intrusion and the defined alteration zones are given in Table 1. The SiO_2

Table 2
Trace element compositions of the fresh and altered parts of the Vrshnik intrusion. the Buchim porphyry Cu-Au deposit. North Macedonia.

		Ba	Ni	Sc	Co	Cs	Ga	Hf	Nb	Rb	Sn	Sr	Ta	Th	U	V	W	Zr	Y	TOT/C	TOT/S	Sr/Y
		ppm																		wt.%		
	MDL	1	20	1	0.2	0.1	0.5	0.1	0.1	0.1	1	0.5	0.1	0.2	0.1	8	0.5	0.1	0.1	0.02	0.02	
Sample	Sample type																					
VS1	Phyllic alteration	965	<20	12	12.6	2.4	18.2	4.4	12	157.4	6	303.8	0.9	45.3	15.9	205	5.2	164.5	30.3	1.34	1.15	10.0
VS6	Argillic alteration	1209	<20	10	7.1	3.4	19.8	6.1	11.3	183.6	2	264.7	0.9	47.7	10.8	130	8.1	223.4	22.8	0.61	0.03	11.6
VS8	Potassic alteration	929	<20	7	14.3	3.2	19	4.8	6.8	152.4	4	307.2	0.7	50.7	8.7	138	7.2	182.1	11.9	0.57	1.05	25.8
VS9	Chlorite alteration	1353	<20	11	18.8	2.7	23.2	4.2	13.2	197.9	5	461.3	0.9	54.8	12.2	102	8.7	154.1	24.4	0.06	1.16	18.9
VSR	Fresh rock	1729	<20	13	14	0.9	18.9	4.9	11.2	110	3	1611.6	1	56.6	14.5	158	2.3	175.7	27.2	0.04	0.02	59.3

		La	Ce	Pr	Nd	Sm	Eu	Gd	Tb	Dy	Ho	Er	Tm	Yb	Lu	ΣREE
	MDL	0.1	0.1	0.02	0.3	0.05	0.02	0.05	0.01	0.05	0.02	0.03	0.01	0.05	0.01	
Sample	Sample type															
VS1	Phyllic alteration	47.6	105.2	12.85	48.3	9	1.69	7.4	1.01	5.24	1	3.11	0.45	2.93	0.45	246.23
VS6	Argillic alteration	71.8	131.4	13.83	50.1	8	1.85	6.08	0.81	4.09	0.78	2.25	0.34	2.31	0.36	294
VS8	Potassic alteration	30.9	60.6	6.58	23.7	3.91	1.05	3.14	0.41	2.1	0.43	1.22	0.18	1.29	0.21	135.72
VS9	Chlorite alteration	125.1	193.5	18.38	59.2	8.44	1.7	6.2	0.79	4	0.78	2.19	0.33	2.19	0.35	423.15
VSR	Fresh rock	75.4	135.7	15.1	54.3	9.39	1.94	7.04	0.93	4.94	0.93	2.58	0.39	2.52	0.4	311.56

		Mo	Cu	Pb	Zn	Ni	As	Cd	Sb	Bi	Ag	Hg	Tl	Se	Au
		ppm													ppb
	MDL	0.1	0.1	0.1	1	0.1	0.5	0.1	0.1	0.1	0.1	0.01	0.1	0.5	0.5
Sample	Sample type														
VS1	Phyllic alteration	3	288.2	264.3	36	5.3	25.7	<0,1	<0,1	1.2	0.8	0.02	0.1	1.8	44.4
VS6	Argillic alteration	0.6	12.1	9.9	42	11.6	1.1	<0,1	<0,1	1.4	<0,1	<0,01	0.2	<0,5	2.8
VS8	Potassic alteration	9.3	1268.8	11.3	18	8	199.5	<0,1	1.5	1.9	0.3	<0,01	0.2	2.7	35.2
VS9	Chlorite alteration	19.2	9675	12.4	40	9.8	27.9	<0,1	0.1	1.6	1.4	0.01	0.3	6.2	1359.5
VSR	Fresh rock	0.3	360.5	9.5	28	4.4	1.4	<0,1	<0,1	1.2	<0,1	<0,01	<0,1	<0,5	0.9

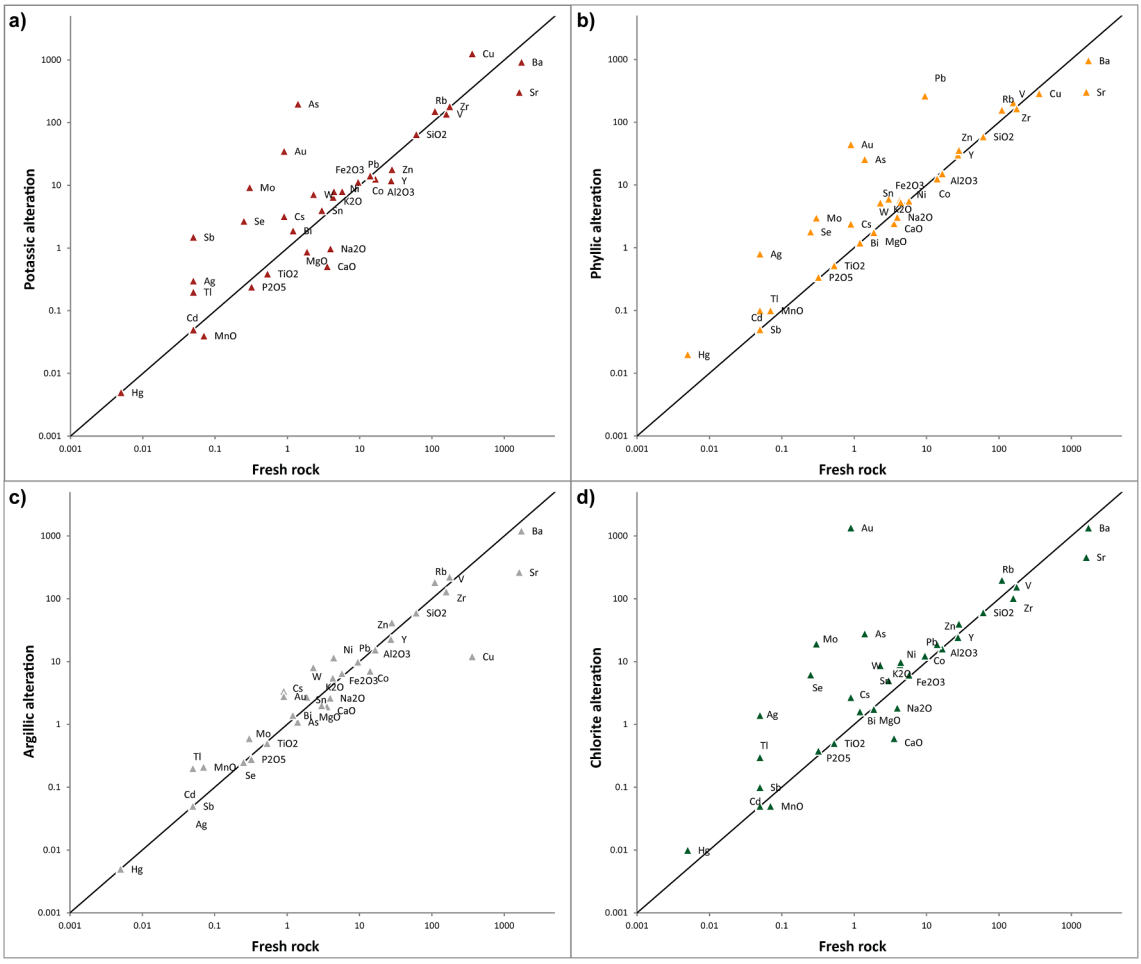

Fig. 10. Isocon diagrams for representative samples from **a)** potassic alteration zone; **b)** phyllic alteration zone; **c)** argillic alteration zone; **d)** chlorite alteration zone of the Vršnik ore body, the Bučim porphyry Cu-Au deposit, North Macedonia.

vs. total alkali contents plot for unaltered and altered samples in the field of trachyte/trachydacite (Fig. 9a). The fresh intrusion has a calc-alkaline character (Fig. 9b) with a strong high-K calc-alkaline to shoshonitic affinity (Fig. 9c; Fig. 9d). Most of the alteration zones have preserved the original calc-alkaline character, except for potassic alteration zone, which shows a significant depletion in the MgO and enrichment in Fe_2O_3 content compared to the fresh protolith (Table 1). Therefore it is moved to the tholeiitic field of the AFM diagram (Fig. 9b). The potassic alteration zone also displays a prominent depletion in Na_2O and CaO and significant enrichment in K_2O compared to the fresh trachyte/trachydacite (Table 1). The phyllic alteration zone resembles well the major-element composition of the fresh protolith except for a decreased CaO content (Table 1). The argillic alteration is characterized by an enrichment in MgO, Fe_2O_3, and K_2O and a depletion in Na_2O and CaO (Table 1). The chlorite alteration zone shows a depletion in Na_2O and CaO and enrichment in K_2O compared to the fresh protolith (Table 1).

The trace element compositions of the analysed rock samples are given in Table 2. Both unaltered and altered samples show an arc-type trace element signature characterized by enrichment in incompatible elements, strong depletions of Nb and Ti, and a pronounced Pb peak (Fig. 9e). The Sr/Y and La/Yb ratios of the fresh trachyte/trachydacite sample is 59 and 30, respectively. All altered samples show lower Sr/Y ratios resulted from a greater mobility of Sr over Y. The La/Yb of the altered samples varies from 16 to 57 (Table 2). All samples are enriched in LREE compared to their HREE concentrations. A negative Eu anomaly has been found in the unaltered trachyte/trachydacite sample as well as in all altered samples (Fig. 9f; Table 2).

Isocon analysis (Grant, 2005), applied to altered and fresh parts of the Vršnik intrusion, revealed that the potassic alteration is followed by enrichment in chalcophile elements, including Cu, Au, Ag, Mo, Se, As, Tl and Sb (Fig. 10a). The phyllic alteration is associated with enrichment in Pb, Zn, Au, Ag, Mo, Hg, Se, As, Tl and Sb, but not in Cu (Fig. 10b). The argillic alteration zone is characterized by a weak enrichment in Au and depletion in Cu compared to the fresh protolith (Fig. 10c). The chlorite alteration is associated with enrichment in a full suite of chalcophile elements, including Cu, Au, Ag, Mo, Hg, Se, As, Tl and Sb (Fig. 10d).

3.4. *Fluid inclusion petrography*

The fluid inclusion study was performed on quartz separated from mineralized quartz veinlets associated with the different alteration zones (Fig. 6) to reconstruct the evolution of fluids responsible for ore deposition and formation of the alteration zones at the Vršnik ore body.

According to the number and the volume proportions of phases present at room temperature, the following types of fluid inclusions were identified. Type 1 fluid inclusions are two-phase, L + V, L-rich inclusions usually contain over 80% of the L phase. They vary in size from < 5 up to 100 μm and in shape from irregular to rounded (Fig. 11a). Type 2 fluid inclusions are two-phase, L + V, V-rich, usually containing <15% of the L phase. Their size is between 25 and 50 μm and exhibit irregular to slightly rounded shapes (Fig. 11b). Type 3 fluid inclusions are three-phase, L + V + S_1, inclusions that contain halite daughter minerals. This type of inclusions mostly has irregular to slightly rounded shapes and the size around 50 μm (Fig. 11c). Type 4 fluid inclusions are

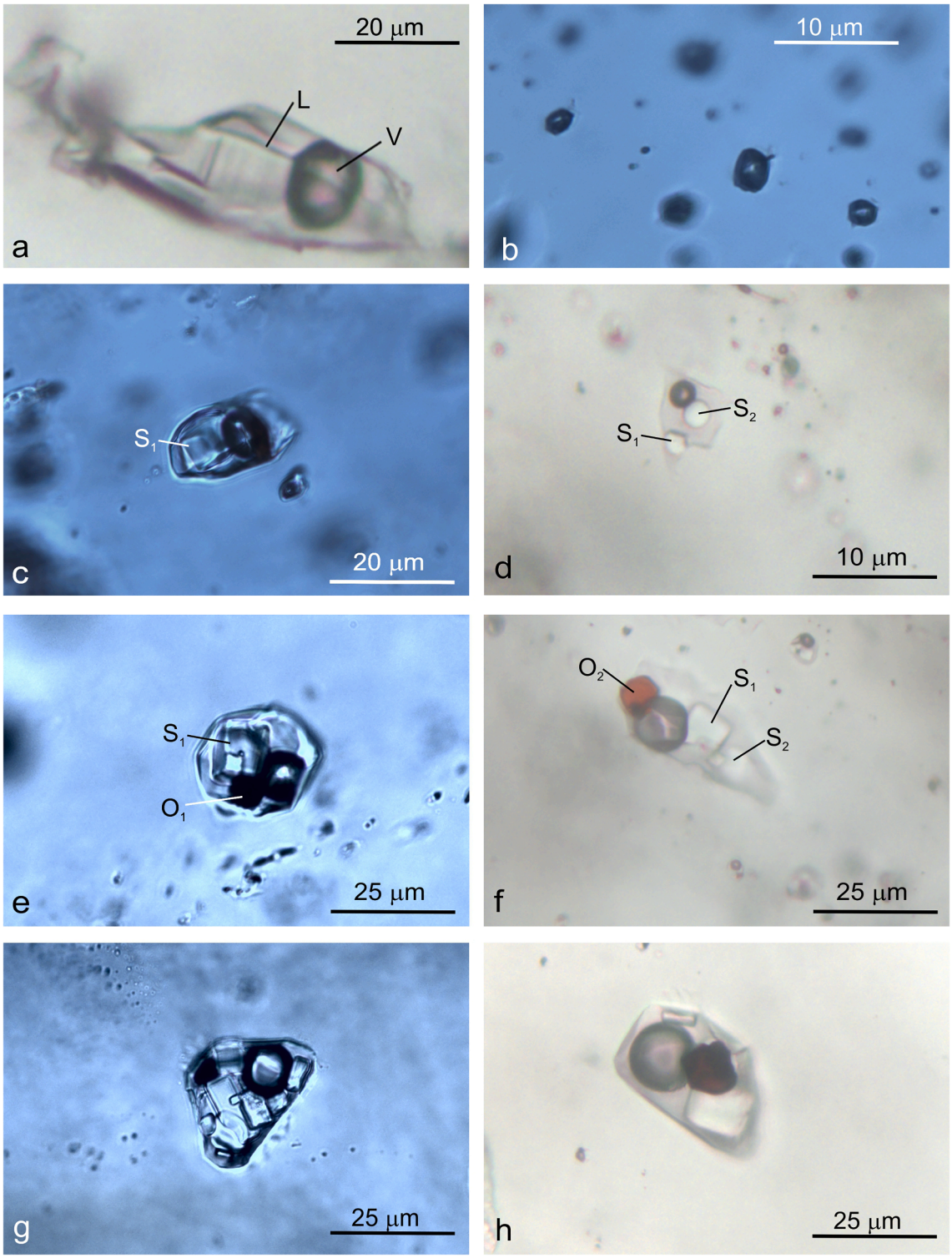

Fig. 11. Microphotographs of seven types of fluid inclusions recognized in quartz associated with the mineralization in the Vršnik ore body, the Bučim porphyry Cu-Au deposit, North Macedonia: **a)** Two phase, L + V, L-rich inclusions; **b)** Two phase, L + V, V-rich inclusions; **c)** Three phase, L + V + S_1, inclusions contain halite daughter minerals; **d)** Poly-phase, L + V + S_n, inclusions contain several (n) daughter minerals; **e)** Poly-phase, L + V + S_1 + O_1, inclusions contain halite and an opaque mineral phase; **f)** Poly-phase, L + V + S_1 + S_2 + O_2, inclusions contain halite and sylvite and red platy hematite; g) Poly-phase, L + V + S_n + O_1, inclusions contain halite, sylvite, unidentified anisotropic daughter minerals and chalcopyrite; **g)** Poly-phase, L + V + S_1 + S_2 + O_2, inclusions contain halite and sylvite and red platy hematite; **h)** Poly-phase, L + V + S_n + O_2, inclusions contain halite, sylvite, unidentified anisotropic daughter minerals and hematite. L = liquid, V = vapour, S_1 = halite, S_2 = sylvite, S_3 = transparent anisotropic solid phase, O_1 = chalcopyrite, O_2 = hematite.

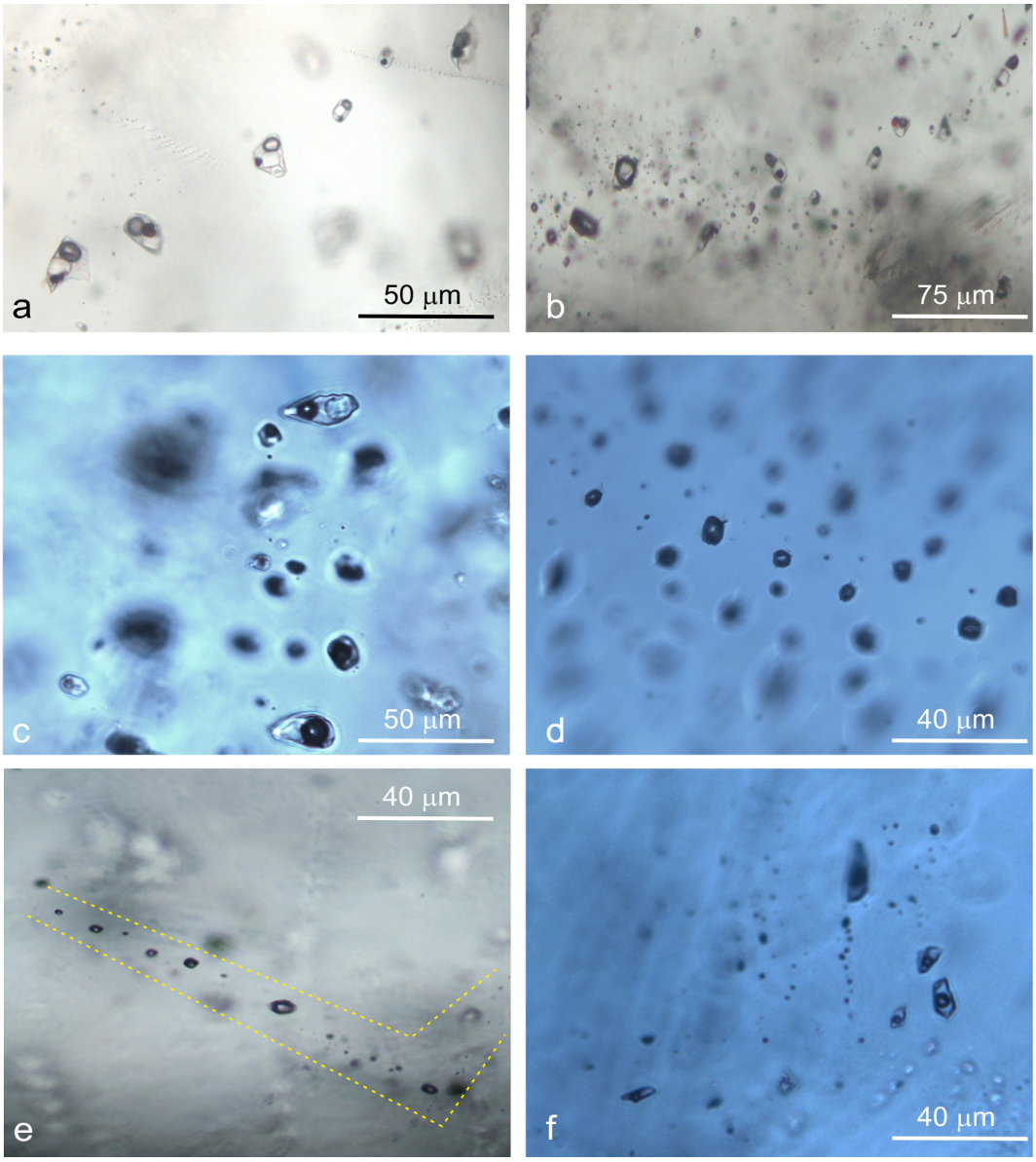

Fig. 12. Microphotographs of fluid inclusion assemblages that represent four main types of fluids recognized in quartz associated with the mineralization in the Vršnik ore body, the Bučim porphyry Cu-Au deposit, North Macedonia: **a)** A fluid inclusion assemblage consisting of aqueous fluid inclusions with transparent daughter minerals and ore minerals (chalcopyrite and/or hematite); **b)** Fluid inclusion assemblages composed of coexisting poly-phase ore mineral-bearing fluid inclusions and two phase V-rich fluid inclusions; **c)** A fluid inclusion assemblage consisting of aqueous fluid inclusions with one or more transparent daughter minerals; **d)** A cluster of vapour rich inclusions; **e)** A growth zone marked by fluid inclusion assemblages composed exclusively of vapour rich inclusions; f) A fluid inclusion assemblages composed of aqueous two-phase L-rich inclusions.

poly-phase, $L + V + S_n$, inclusions that contain several daughter minerals, including halite and sylvite. This type of inclusions also come in irregular to slightly rounded shapes and their size rarely exceeds 10 μm (Fig. 11d). Type 5 fluid inclusions are poly-phase, $L + V + S_1 + O_1$, with halite and an opaque mineral, most probably chalcopyrite. This type of inclusions come in elongated shapes with their sizes up to 50 μm (Fig. 11e). Type 6 fluid inclusions are poly-phase, $L + V + S_1 + S_2 + O_2$, inclusions that contain halite and sylvite as well as a red platy hematite crystal. This type of inclusions usually come in slightly rounded shapes with the size up to 50 μm (Fig. 11f). Type 7 fluid inclusions are poly-phase, $L + V + S_n + O_1 \pm O_2$, inclusions with halite, sylvite and unidentified anisotropic daughter minerals. They also contain chalcopyrite and/or hematite. This type of inclusions also usually have elongated shapes and range in sizes up to 50 μm (Fig. 11g,h).

Petrographic characteristics and spatial distribution of fluid inclusion assemblages suggest four main stages in the evolution of fluids in the Vršnik ore body: Stage 1) Fluid inclusion assemblages consist of aqueous fluid inclusions that contain one or more transparent daughter minerals accompanied with ore minerals (chalcopyrite and/or hematite; Types 5, 6 and 7). Some of the fluid inclusion assemblages also contain vapour-rich inclusions (Type 2) with a degree of fill varying between 5 and 15%. The fluid inclusion assemblages that represent Stage 1 can be found as isolated clusters or along growth zones (Fig. 12a,b).

Stage 2) Fluid inclusion assemblages contain aqueous inclusions with one or more transparent isotropic daughter minerals but ore minerals (chalcopyrite and/or hematite) are absent (Types 3 and 4). These types of fluid inclusion assemblages occur as clusters or distributed along trails (Fig. 12c).

Stage 3) Fluid inclusion assemblages consist exclusively of vapour rich inclusions (Type 2) with the degree of fill $< 5\%$. They are found within larger clusters, along growth zones and along healed fractures (Fig. 12d,e).

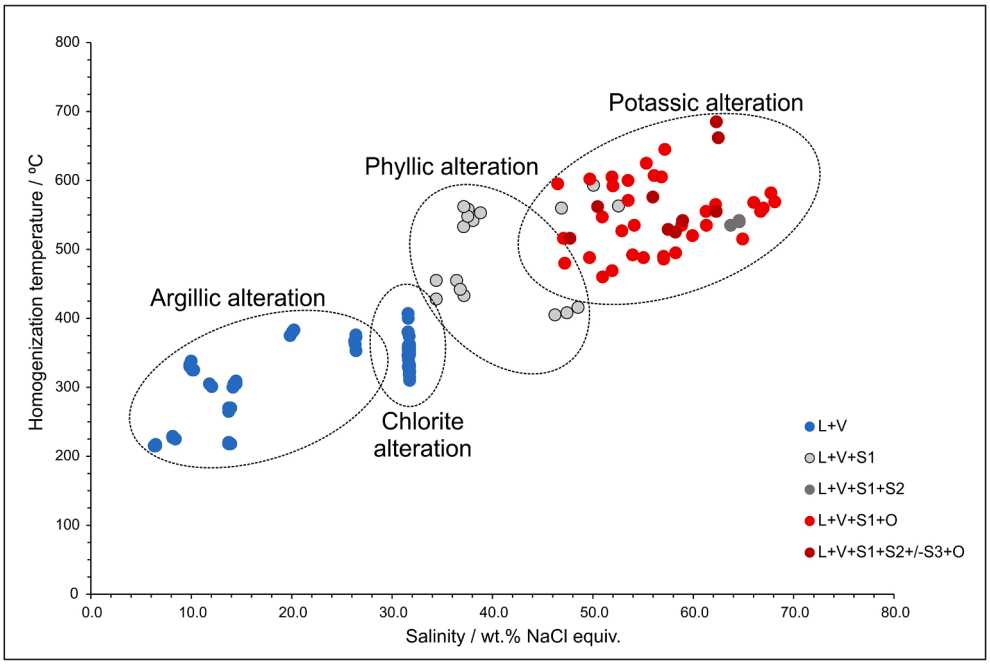

Fig. 13. Correlation of homogenization temperature and salinity for fluid inclusions hosted by quartz-carbonate veinlets associated with different alteration zones of the Vršnik ore body, the Bučim porphyry Cu-Au deposit, North Macedonia.

Table 3
Carbon and oxygen isotope composition of carbonates from the Vršnik ore body, the Bučim porphyry Cu-Au deposit, North Macedonia.

				$\delta^{13}C$	$\delta^{18}O$	$\delta^{18}O$
				(‰; VPDB)	(‰; VPDB)	(‰; VSMOW)
C2	VS7	Calcite	potassic → chlorite	−1.7	−17.7	12.7
C3	VS14	Siderite	potassic → chlorite	−1.5	−9.0	21.6
C4	VS19	Siderite	potassic → argillic	2.0	−6.5	24.2
C5	VS12	Calcite	potassic → chlorite	−1.3	−15.1	15.3
C6	VS6	Calcite	phyllic	−1.6	−21.2	9.1
C7	VS7	Calcite	potassic → chlorite	−1.3	−16.9	13.5
C8	VS1	Calcite	phyllic	−1.3	−17.5	12.9
C9	VS19	Siderite	potassic → argillic	−1.3	−17.2	13.2
C10	VS19	Siderite	potassic → argillic	1.5	−10.3	20.3
C11	VS14	Siderite	potassic → chlorite	−7.2	−9.4	21.3
C12	VS12	Siderite	potassic → chlorite	−3.2	−15.0	15.5

Stage 4) Fluid inclusion assemblages are composed of aqueous two-phase (L + V) inclusions (Type 1). This is the most common type of fluid inclusion assemblages. They are usually disseminated as smaller clusters or occur along healed fractures (Fig. 12f).

3.5. Fluid inclusion microthermometry

The microthermometric data are summarized in Fig. 13 and the complete data set is listed in Appendix 1. Prior to the microthermometric measurements, Raman spectroscopy analysis was performed on representative fluid inclusions. Except for water, the presence of other volatiles, including CO_2, has not been confirmed.

During heating of ore-bearing fluid inclusions (inclusions of types 5, 6, and 7), sylvite always dissolves at lower temperatures than halite, and halite dissolves before the vapour disappearance. Several fluid inclusion assemblages characterized by near-simultaneous vapour and halite disappearance have been observed as well. Numerous inclusions decrepitated after the halite dissolution but before the vapour disappearance. Ore minerals (chalcopyrite and hematite), as well as the anisotropic daughter mineral (S_3, most probably anhydrite), have not been dissolved even at temperatures as high as 1000 °C. The bulk salinity of ore-bearing fluid inclusion assemblages ranges between 34.9

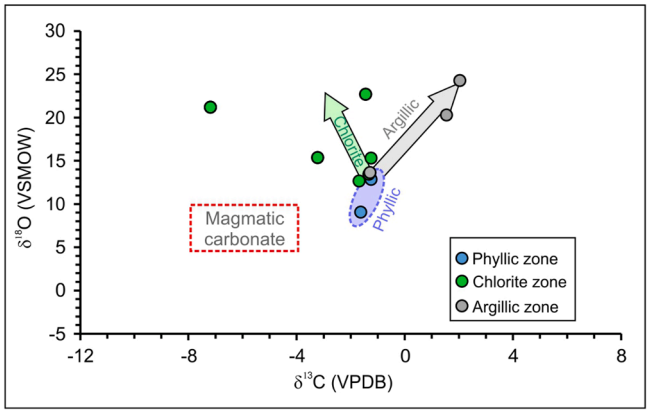

Fig. 14. $\delta^{13}C$ vs. $\delta^{18}O$ plot of carbonates from different alteration zones of the Vršnik ore body, the Bučim porphyry Cu-Au deposit, North Macedonia. Reference values for magmatic carbonates are from Taylor et al. (1967).

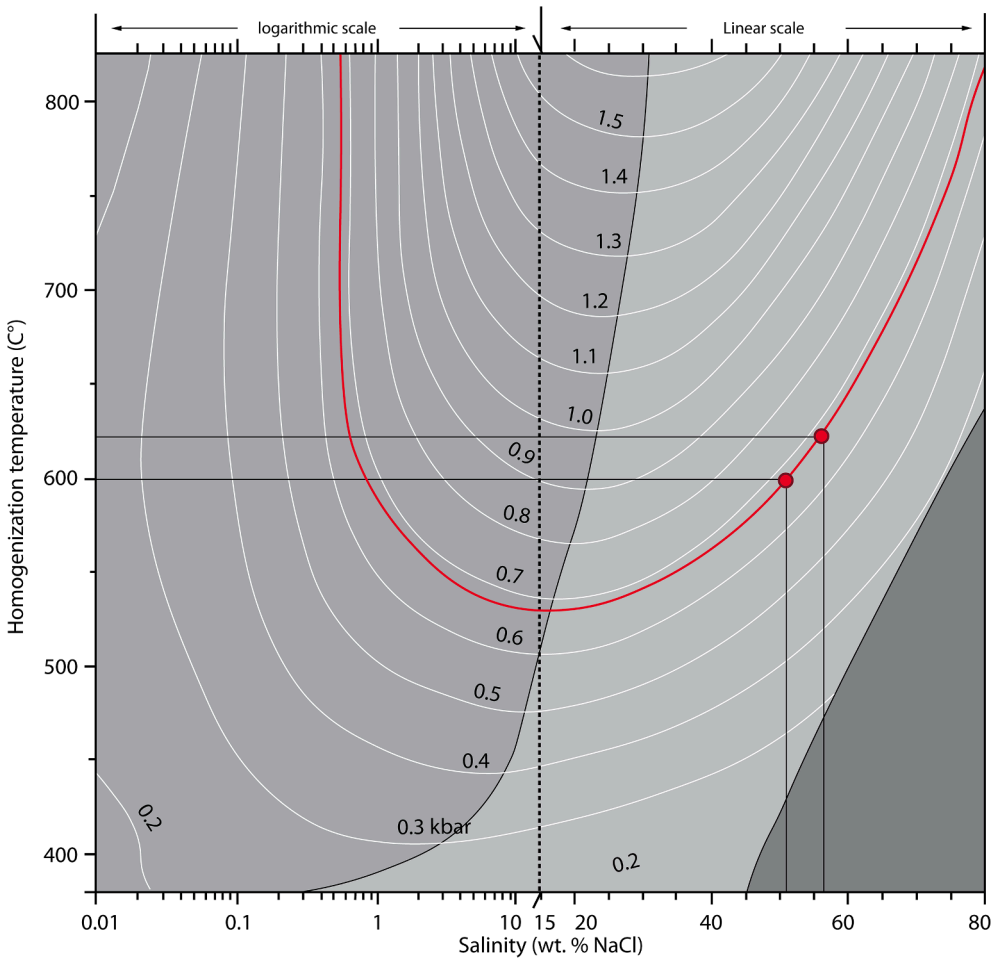

Fig. 15. Entrapping conditions of coexisting poly-phase ore-bearing (high-density) and V-rich (low-density) fluid inclusions estimated based on microthermometric properties of the high-density fluid inclusions. The homogenization temperature-salinity-pressure diagram for a H_2O-NaCl system is adopted from Klyukin et al. (2019).

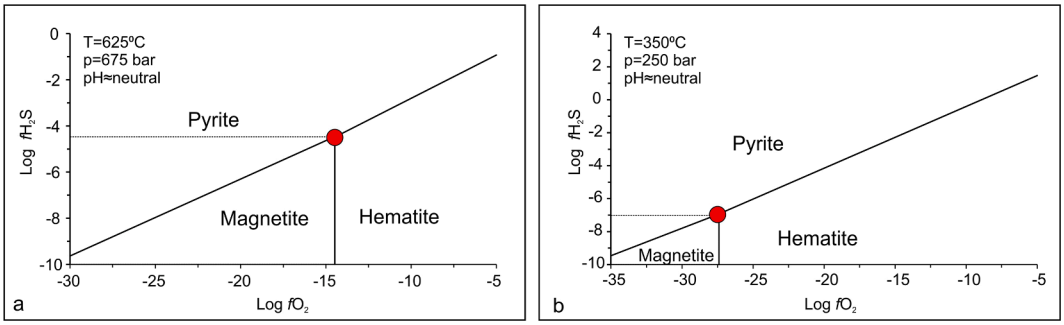

Fig. 16. Stability of hematite, magnetite and pyrite in the log fO_2 vs. log fH_2S field constructed for **a)** Ore-forming conditions associated with development of the potassic alteration zone and **b)** Deposition of the sulfide mineralization in the chlorite alteration zone of the Vršnik ore body, the Bučim porphyry Cu-Au deposit, North Macedonia. The thermodynamical modelling was preformed using the SUPCRT model and the associated databases (Johnson et al. 1992).

and 73.5 wt% NaCl equiv. (Appendix 1). The assemblage with the lowest recorded homogenization temperature (T_h = 466 ± 6 °C, n = 3) has a salinity between 51.0 and 51.9 wt% NaCl equiv. and the bulk density of 1.072 ± 0.002 g/cm^3. The assemblage with the highest recorded T_h (674 ± 16 °C, n = 5) displays a salinity of 61.8 ± 6.6 wt% NaCl equiv. and the density of 1.053 ± 0.018 g/cm^3. Vapour-rich two-phase inclusions have been found in several ore-bearing fluid inclusion assemblages. Although phase transitions in this type of inclusion have not been recorded, their presence suggests the phase separation of high-salinity and high-density Cu- and Fe-bearing fluids from low-salinity and low-density fluids. In addition, the homogenization temperatures of the ore-bearing fluid inclusions from this type of fluid inclusion assemblages (600–645 °C; Appendix 1) may be considered as the entrapment temperature (e.g., Roedder, 1984; Bodnar, 2003).

Halite-saturated and ore mineral-free fluid inclusions (types 3 and 4) are characterized by halite dissolution preceding the total homogenization. The total homogenization to the liquid phase was recorded in the interval between 342 ± 19 to > 600 °C. Numerous fluid inclusions decrepitated prior the total homogenization. The bulk salinity calculated from the halite dissolution temperature ranges from 29.5 to 64.3

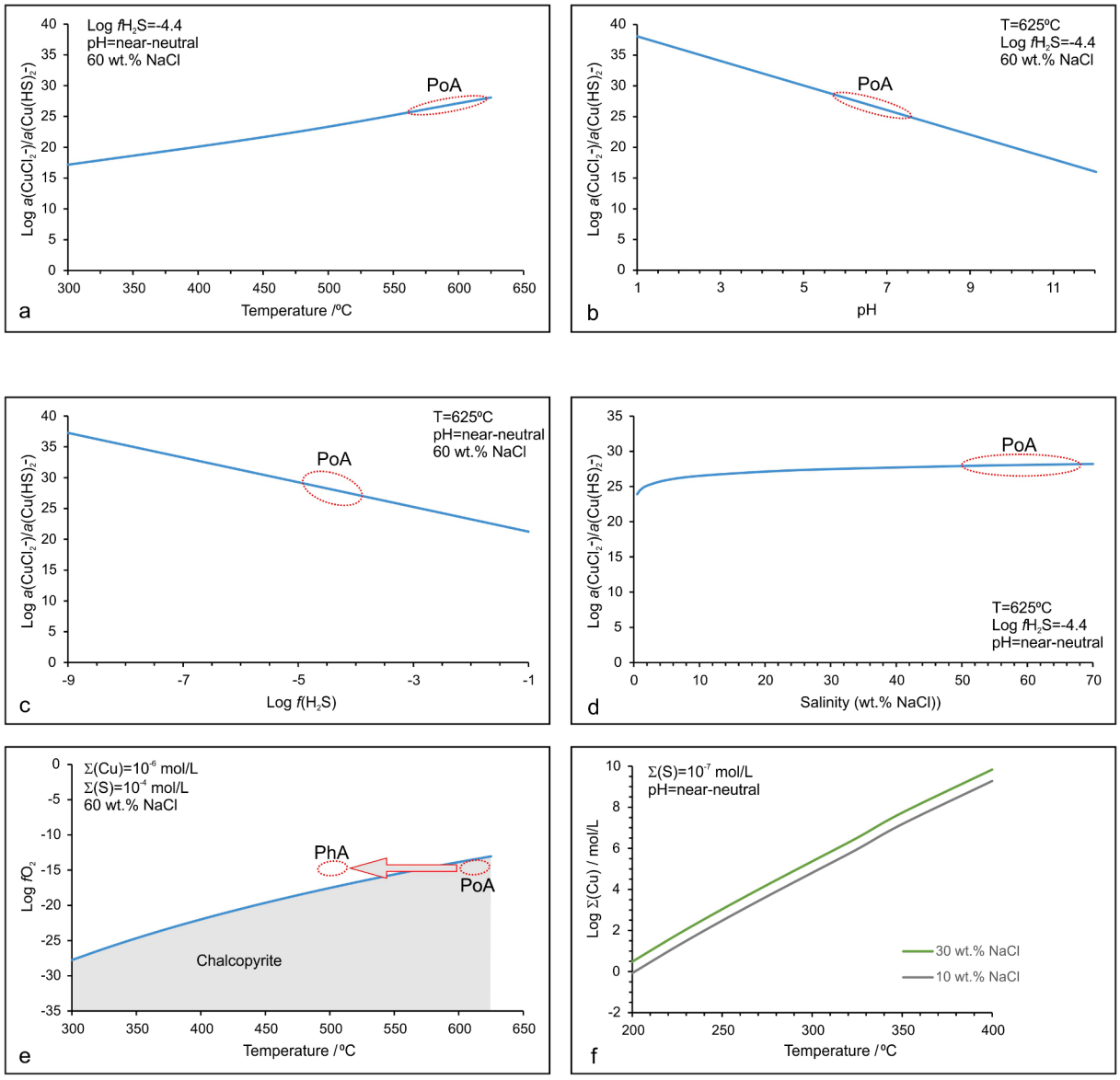

Fig. 17. Diagram showing **a)** the $CuCl_2^-/Cu(HS)_2^-$ ratio over a wide temperature range assuming fH_2S of $10^{-4.4}$ bar (coexistence of hematite, magnetite and pyrite), fluid salinity of 60 wt% NaCl and near-neutral pH conditions; **b)** the $CuCl_2^-/Cu(HS)_2^-$ ratio over a wide pH range assuming fH_2S of $10^{-4.4}$ bar, temperature of 625 °C and fluid salinity of 60 wt% NaCl; **c)** the $CuCl_2^-/Cu(HS)_2^-$ ratio over a wide fH_2S range assuming temperature of 625 °C, fluid salinity of 60 wt% NaCl and near-neutral pH conditions; **d)** the $CuCl_2^-/Cu(HS)_2^-$ ratio over a wide salinity range assuming temperature of 625 °C, fH_2S of $10^{-4.4}$ bar and near-neutral pH conditions; **e)** stability of chalcopyrite in the log fO_2 vs. temperature field assuming $\Sigma(Cu) = 10^{-6}$ mol/L, $\Sigma(S) = 10^{-4}$ mol/L, fluid salinity of 60 wt% NaCl and the Fe activity buffered by magnetite and hematite; f) solubility of Cu in forms of Cu-chloride complexes under the P-T-x conditions estimated for the chlorite alteration zone. The thermodynamical modelling was preformed using the SUPCRT model and the associated databases (Johnson et al. 1992). The thermodynamical properties of Cu-chloride and bisulfide complexes are adopted from Sverjensky et al. (1997) and Mountain and Seward (2003), respectively. The conditions estimated for the potassic and phyllic alteration zones are marked as PoA and PhA, representatively.

wt% NaCl equiv. The bulk density varies between 0.815 and 1.207 g/cm^3.

Fluid inclusion assemblages composed exclusively of vapour-rich inclusions type 2 do not show any phase transitions in the temperature range between −180 and +600 °C and therefore their salinities and densities remain unknown. Several fluid inclusion assemblages were a subject of massive decrepitation at temperatures around 450 °C.

The type 1 two-phase liquid-rich inclusions are characterized with homogenization to the liquid phase in the temperature interval from 216 ± 1 to 390 ± 13 °C. The eutectic temperature was recorded for several fluid inclusion assemblages. The values around −52 °C suggest a $CaCl_2$-NaCl-H_2O system (Vanko et al, 1988). In the great majority of the two-phase liquid-rich inclusions hydrohalite has been recognized as the last melting phase. Its melting temperature between −28.5 and −21.0 °C suggests the bulk salinity around 31.6 wt% NaCl equiv., assuming the $CaCl_2$-NaCl-H_2O system (Steele-MacInnis et al., 2011). Several two-phase liquid-rich fluid inclusions showed the hydrohalite-halite phase transition around 0 °C and the dissolution of halite between 5.1 and 22.0 °C reflecting the bulk salinity of ~ 26.4 wt% NaCl equiv. The rest of two-phase liquid-rich inclusions are characterized by ice as the last melting phase. The ice melting temperature between −17.0 and −3.9 °C reflects the bulk salinity in the range from 6.3 up to 20.2 wt% NaCl equiv.

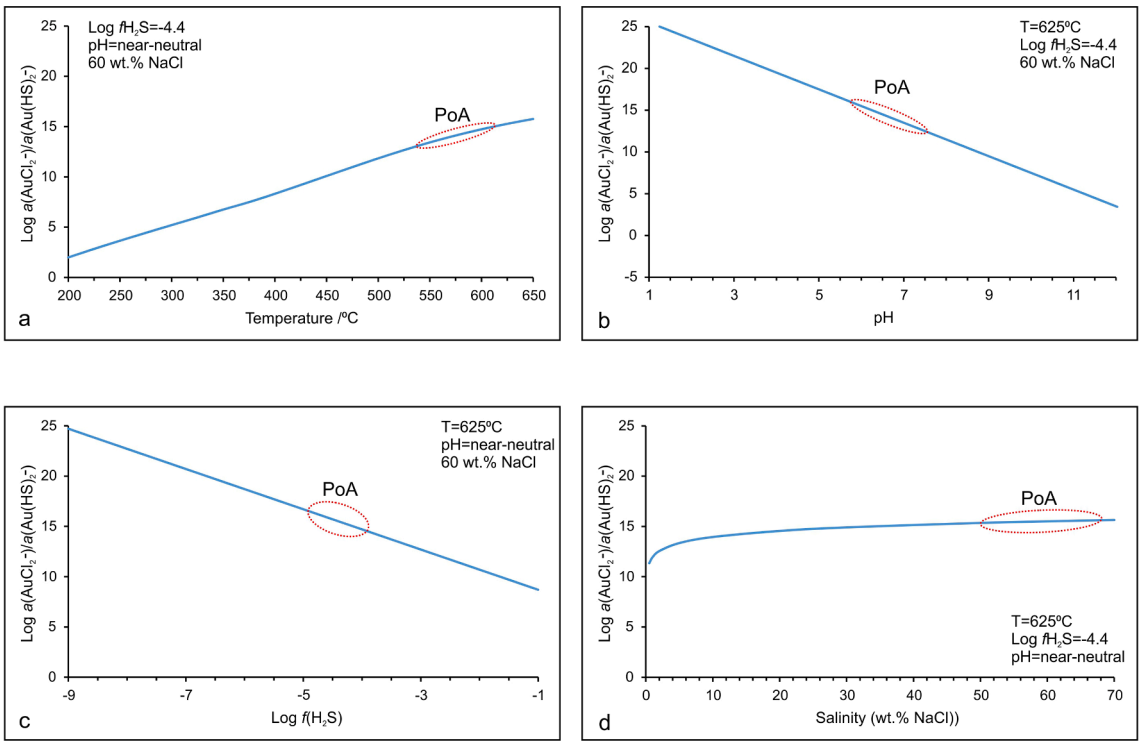

Fig. 18. Diagram showing the $AuCl_2^-/Au(HS)_2^-$ ratio over **a)** a wide temperature range assuming fH_2S of $10^{-4.4}$ bar (coexistence of hematite, magnetite and pyrite), fluid salinity of 60 wt% NaCl and near-neutral pH conditions; **b)** a wide pH range assuming fH_2S of $10^{-4.4}$ bar, temperature of 625 °C and fluid salinity of 60 wt% NaCl; **c)** a wide fH_2S range assuming temperature of 625 °C, fluid salinity of 60 wt% NaCl and near-neutral pH conditions; **d)** a wide salinity range assuming temperature of 625 °C, fH_2S of $10^{-4.4}$ bar and near-neutral pH conditions. The thermodynamical modelling was preformed using the SUPCRT model and the associated databases (Johnson et al. 1992). The thermodynamical properties of Au-bisulfide and Au-chloride complexes are adopted from Sverjensky et al. (1997). The conditions estimated for the potassic and phyllic alteration zones are marked as PoA and PhA, representatively.

3.6. Stable isotope data

The $\delta^{13}C$ and $\delta^{18}O$ values from the carbonates associated with the mineralized veinlets are listed in Table 3. The $\delta^{13}C$ and $\delta^{18}O$ values of calcite range between −1.7 and −1.3 ‰ VPDB and 9.1 and 15.3 ‰ VSMOW, respectively. The $\delta^{13}C$ and $\delta^{18}O$ values of siderite range between −1.7 and 2.0 ‰ VPDB and 13.2 and 24.2 ‰ VSMOW, respectively. Calcite from the phyllic alteration zone shows a contribution of magmatic CO_2. Carbonates separated from quartz-carbonate veinlets in the argillic alteration zone are characterized with an enrichment in ^{13}C and ^{18}O. In contrast, carbonates separated from the chlorite zone show an enrichment in ^{18}O and a broad range of $\delta^{13}C$ values (Fig. 14).

4. Discussion

The Vršnik intrusion, like other basaltic to trachyandesitic rocks of the Oligocene/Early Miocene age along the Balkan Peninsula (e.g., Serafimovski et al., 2010; Borojević Šoštarić et al., 2012; Strmić Palinkaš et al., 2016; Strmić Palinkaš et al., 2018a) displays a high-K calc-alkaline to shoshonitic character, enrichment in LILE, depletion in HFSE and relatively high Sr/Y and La/Yb ratios (Table 1, Fig. 9). This type of geochemical signature is attributed to delamination of the lithospheric root and partial melting of lithospheric domains that have previously been metasomatosed in a subductional setting (Cvetković et al., 2004; Richards, 2009; Perkins et al., 2018) and, together with the known radiometric age ($^{206}Pb/^{238}U$ age of 24.42 ± 0.52 and 24.44 ± 0.49 Ma; Lehmann et al., 2013), suggests the post-collisional origin of the Vršnik intrusion and the associated porphyry Cu-Au mineralization.

Porphyry deposits are products of an interaction of fluids exsolved from cooling, water-rich, oxidized calc-alkaline magmas with subvolcanic plutons of an intermediate to felsic composition at depths of approximately 2–6 km (Sinclair, 2007; Sillitoe, 2010; Cooke et al., 2014). The fluid/rock interaction results with the ore deposition as well as with development of three-dimensional halo of hydrothermal alteration assemblages within and around the subvolcanic complex (e.g., Cooke et al., 2014). Therefore, mineralogical and geochemical characteristics of hydrothermal alteration zones are often used as proxies for reconstruction of physicochemical properties of the mineralizing fluids in porphyry systems (e.g., Lowell and Guilbert, 1970; Ulrich and Heinrich, 2002; Cannell et al., 2005).

The potassic alteration zone of the Vršnik ore body (Figs. 4 and 6) is characterized by the replacement of amphibole with biotite and crystallization of hydrothermal biotite, magnetite, and hematite within the fine-grained groundmass of the intrusion (Figs. 4 and 5c). Oxidation of ferrous to ferric iron during the formation of potassic alteration assemblage may promote reduction of sulfur species in the mineralizing fluids (from SO_4^{2-} to $H_2S(aq)$) and therefore trigger deposition of sulfide minerals, including chalcopyrite (Fontboté et al., 2017; Watanabe et al., 2018). Alternatively, the sulfate reduction may occur earlier, due to crystallization of magnetite in an oxidized silicate melt and the formed sulfide is transported by exsolved magmatic fluids (e.g., Sun et al., 2015). The isocon analysis (Fig. 10a) suggests that, in addition to Cu, the fluids associated with the formation of the potassic alteration zone also introduced other chalcophile elements, including Au, Ag, Mo, Se, As, Tl and Sb.

Although multiple magmatic-hydrothermal overprints usually complicate the interpretation of fluid inclusion data in porphyry deposits (e.g., Rusk et al., 2008), the Vršnik ore body is somewhat different because it represents the youngest intrusion in the Bučim deposit and therefore has not been affected by later magmatic activities. Fluid inclusion data obtained from the preserved potassic alteration zone (samples VS13 and VS15; Fig. 6) may give an insight into physicochemical characteristics of ore-bearing fluids. The fluid inclusion study suggests that the potassic alteration zone represents a result of

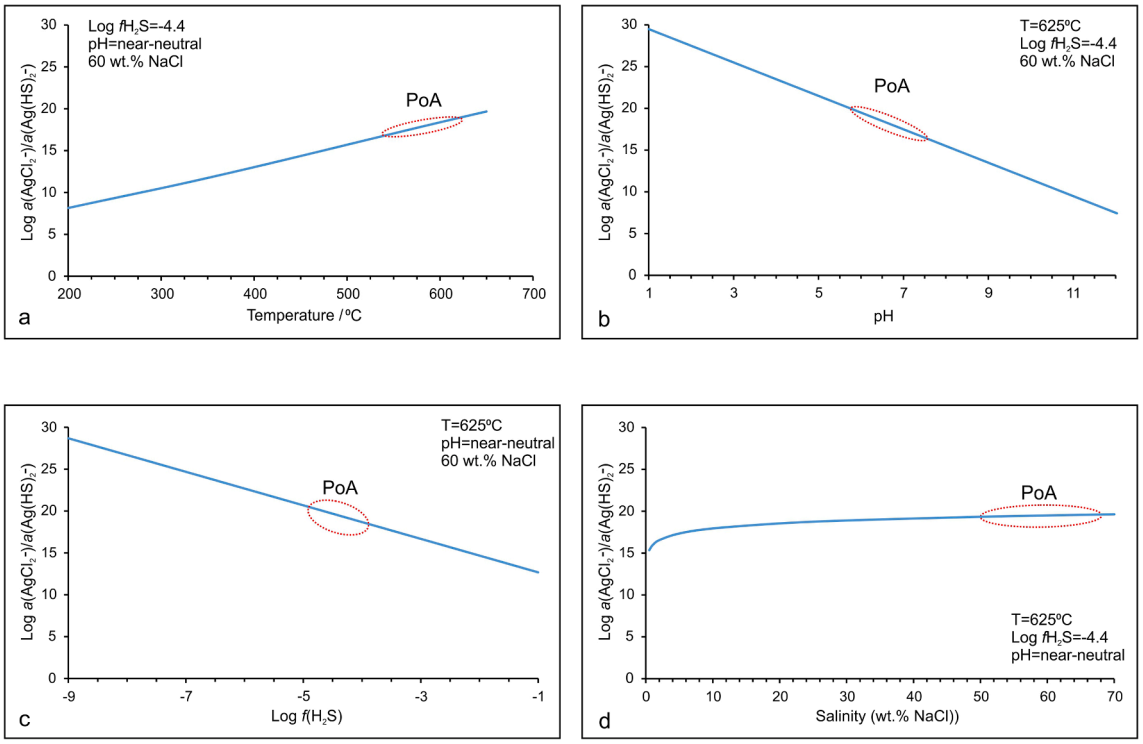

Fig. 19. Diagram showing the $AgCl_2^-/Ag(HS)_2^-$ ratio over **a)** a wide temperature range assuming fH_2S of $10^{-4.4}$ bar (coexistence of hematite, magnetite and pyrite), fluid salinity of 60 wt% NaCl and near-neutral pH conditions; **b)** a wide pH range assuming fH_2S of $10^{-4.4}$ bar, temperature of 625 °C and fluid salinity of 60 wt% NaCl; **c)** a wide fH_2S range assuming temperature of 625 °C, fluid salinity of 60 wt% NaCl and near-neutral pH conditions; **d)** a wide salinity range assuming temperature of 625 °C, fH_2S of $10^{-4.4}$ bar and near-neutral pH conditions. The thermodynamical modelling was preformed using the SUPCRT model and the associated databases (Johnson et al. 1992). The thermodynamical properties of Au-bisulfide and Au-chloride complexes are adopted from Sverjensky et al. (1997). The conditions estimated for the potassic and phyllic alteration zones are marked as PoA and PhA, respectively.

infiltration of highly saline metal-rich aqueous solutions (fluid inclusions of Types 5, 6 and 7) through the Vršnik intrusion and the surrounding Precambrian gneisses (Fig. 2). The microthermometric data obtained from the fluid inclusion assemblages that consist of coexisting high-density (ore-bearing poly-phase) and low-density (V-rich) inclusions (e.g., FIA#8 and FIA#16, Appendix 1) reveal their entrapment at temperatures between 600 and 645ºC and the pressure of approximately 0.675 kbar (Fig. 15). The estimated pressure corresponds to the depth of approximately 2.5 km, assuming lithostatic conditions. The coexistence of pyrite, magnetite, and hematite in the mineral paragenesis reflects the H_2S and oxygen fugacity of −4.4 and −14.5, respectively, assuming near-neutral pH conditions (Fig. 16a). The thermodynamic modelling indicates that, in the estimated P-T-x conditions, both Cu and Au were transported in forms of chloride complexes (Fig. 17a-d and 18). Silver was also transported as Ag-chloride (Fig. 19) while other chalcophile elements (Mo, As, Tl, and Sb) were probably introduced in forms of their OH-complexes (Seward et al., 2014).

The phyllic alteration zone (Figs. 4 and 6) is characterized by sericitization of plagioclase and replacement of amphiboles by quartz (Fig. 5f). This alteration zone is barren in terms of copper (Fig. 10b). Its superimposed position over the earlier potassic alteration zone hinders a clear link between the obtained fluid inclusion data and alteration processes. For a long time, it has been accepted that phyllic alteration represents a product of mixing of relatively cold and diluted magmatic fluids with meteoric water (e.g., Reynolds and Beane, 1985; Taylor, 1997). Anyhow, some of more recent studies provide evidence that fluids involved in the formation of phyllic alteration assemblages are rather high-temperature saline magmatic fluids (e.g., Harris and Golding, 2002; Rusk et al., 2008; Kouzmanov and Pokrovski, 2012). The isotope composition of calcite separated from the phyllic alteration zone of the Vršnik ore body points to a contribution of magmatic CO_2 (Fig. 14).

Sericitization and silicification in the phyllic alteration zone of the Vršnik ore body reflect relatively acid conditions that may have a role in the cease of the Cu deposition. However, the mineral paragenesis suggests that, in contrast to potassic alteration processes, phyllic alteration was not associated with oxidation of ferrous to ferric iron that has been recognized as an efficient mechanism for reduction of S species in porphyry environments (Fontboté et al., 2017; Watanabe et al., 2018). Therefore, the lack of Cu mineralization in the phyllic alteration zone could be a result of infiltration of high-temperature, saline, and oxidized fluids that kept their Cu-transport capability despite the phyllic alteration processes. The thermodynamic modelling suggests that cooling under steady redox conditions also may promote the mobility of Cu in highly saline Cu- and sulfate-bearing fluids (Fig. 17e).

The argillic and chlorite alteration zones are mostly superimposed on previous potassic alterations (Fig. 6). Both argillic and chlorite alteration assemblages (Fig. 4) reflect infiltration of near-neutral to slightly acid fluids and a high water/rock ratio. The complete loss of the original porphyritic texture in ***the chlorite zone*** suggests a particularly high water/rock ratio in the portion of the system affected by chloritization. Chloritization is mostly developed along the contact between the magmatic intrusion and surrounding gneisses (Fig. 6), indicating that this lithological boundary channelled fluids particularly well. The high water/rock ratio as well as a decrease in fluid salinity (e.g., FIA#1-FIA#5; salinity≈30 wt% NaCl; T_H = 310–407ºC; Fig. 13) indicate incursion of meteoric water, probably initiated by the ductile-to-brittle transition due to cooling of the system below 400ºC (Fournier, 1999; Strmić Palinkaš et al., 2014; Strmić Palinkaš et al., 2018a). In addition, the presence of V-only fluid inclusion assemblages (Fig. 12d,e) points to fluid flashing (Moncada and Bodnar, 2012; Simpson et al., 2015) that also can be related to a sudden decompression of the system from the lithostatic to hydrostatic regime (Strmić Palinkaš et al., 2016). The steady $\delta^{13}C$ composition of calcite from the chlorite alteration zone

around −1.5‰ (Table 3, Fig. 14) indicates the magmatic degassing as an important source of CO_2 during the chloritization processes. Anyhow, the increasing $\delta^{18}O$ values reflect a pronounced oxygen isotope fractionation in a cooling hydrothermal system.

The coexistence of pyrite, magnetite, and hematite in the chlorite alteration zone points to the H_2S and oxygen fugacity of −7.0 and −27.4, respectively, assuming temperatures around 350ºC and the pressure of 0.250 kbars (Fig. 16b). Under the estimated P-T-x conditions Cu, Au and Ag are transported as chloride complexes (Figs. 17-19) while other chalcophile elements, such as Mo, As, Sb and Tl, are rather transported as their OH-complexes (e.g., Seward et al., 2014; Simpson et al., 2015; Strmić Palinkaš et al., 2018b). The pronounced cooling (from ≈400ºC down to ≈300ºC, Fig. 13) may have significantly affected the metal-transport capability of the hydrothermal fluids and resulted in deposition of the full suite of chalcophile elements (Fig. 10d; Fig. 17f).

Compared to the chlorite alteration zone, ***the argillic alteration zone*** reflects a lower water/rock ratio. The fluid inclusion data, collected from the quartz-carbonate veinlets in this alteration zone, suggest that earlier potassic alteration assemblages were overprinted by diluted (FIA#37–44; 6.3–20.2 wt% NaCl equiv.) and relatively cold (T_H = 215-383ºC) fluids. The fluid inclusion salinity vs. T_H diagram (Fig. 13) as well as the isotope composition of carbonates (Fig. 14) show mixing trends and suggest an increasing contribution of meteoric water and CO_2. The argillic alteration zone is depleted in most of chalcophile elements, except for Au (Fig. 10c), reflecting a declined capability for metal transport resulted from cooling and dilution of hydrothermal fluids prior or during the early stage of argillitization processes.

5. Conclusions

The geochemical signature of the Vršnik intrusion and its previously published age data suggest that the Bučim porphyry Cu-Au deposit, including the Vršnik ore body, represents a product of the Oligocene/Early Miocene post-collisional magmatic activity. The Vršnik intrusion, as the youngest intrusion in the Bučim deposit, has not been exposed to later magmatic overprints and therefore represents an ideal locality to study the evolution of ore-forming fluids in porphyry Cu-Au systems.

The Cu-Au mineralization is associated with hydrothermal alteration assemblages within and around the Vršnik intrusion. Based on their mineralogical features, the following alteration zones have been identified: 1. potassic; 2. phyllic; 3. chlorite, and 4. argillitic. The potassic and chlorite alteration zones host the Cu-Au mineralization, while the phyllic and argillic zones represent a barren part of the system.

Mineralogical, geochemical, and fluid inclusion data indicates that the potassic alteration zone was developed under the influence of hot, near-neutral, oxidized, and highly saline metal-rich aqueous solutions. Fluid inclusion assemblages composed of coexisting ore mineral-bearing fluid inclusions and V-rich inclusions revealed the formation temperature and pressure of 600-625ºC and 0.675 kbar, respectively. The estimated formation depth was 2.5 km, assuming lithostatic conditions. The oxidation of ferrous to ferric iron in this alteration zone has been recognized as a possible trigger for sulfate reduction and the consequent deposition of sulfide minerals, including chalcopyrite.

The phyllic alteration zone is barren in Cu, although it represents a product of infiltration of hot and saline fluids with a high metal-transport capability. Anyhow, sericitization and silicification suggest a decreased pH value that might have played a significant role in preventing Cu sulfide deposition. The stable isotope composition of carbonates associated with the phyllic alteration zone reveals a contribution of magmatic CO_2.

The chlorite alteration zone is particularly well developed along the contact between the intrusion and surrounding gneisses and reflects a high water/rock ratio. The fluid inclusion assemblages composed exclusively of V-rich inclusions indicate fluid flashing, probably associated with the transition from the lithostatic to hydrostatic regime at the point when the system cooled down to approximately 400ºC. The fluid inclusion assemblages composed of L + V inclusions point to dilution and cooling probably associated with a certain degree of mixing of ore-bearing fluids with meteoric water. The decrease in fluid temperature and salinity resulted with the reduced mobility of metals transported in forms of their chloride complexes, including Cu, Au, and Ag.

The argillic alteration zone was developed under the influence of relatively cold and diluted fluids, with very limited capability for transporting metals. The water/rock ratio was relatively high but lower comparing the chlorite alteration zone.

Declaration of Competing Interest

The authors declare that they have no known competing financial interests or personal relationships that could have appeared to influence the work reported in this paper.

Acknowledgements

We would like to thank the staff at the Bučim mine and in particular Mr. Kiril Filev, the chief geologist, for all support during the field activities. Dr. Kai Nuefeld is thanked for his help in obtaining the SEM data. Constructive reviews by two anonymous reviewers helped to improve the manuscript and are greatly appreciated.

The study was funded by the project A31566 at UiT The Arctic University of Norway. The field work activities of I.P. were funded by an Erasmus internship grant. The research stay at UiT The Arctic University of Norway for I.J. was funded by an Erasmus internship grant.

Appendix A. Supplementary data

Supplementary data to this article can be found online at https://doi.org/10.1016/j.oregeorev.2022.104913.

References

Antić, M.D., Kounov, A., Trivić, B., Wetzel, A., Peytcheva, I., Von Quadt, A., 2016a. Alpine thermal events in the central Serbo-Macedonian Massif (southeastern Serbia). Int. J. Earth Sci. 105 (5), 1485–1505. https://doi.org/10.1007/s00531-015-1266-z.

Antić, M., Peytcheva, I., Von Quadt, A., Kounov, A., Trivić, B., Serafimovski, T., Tasev, G., Gerdjikov, I., Wetzel, A., 2016b. Pre-Alpine evolution of a segment of the North-Gondwanan margin: Geochronological and geochemical evidence from the central Serbo-Macedonian Massif. Gondwana Res. 36, 523–544. https://doi.org/10.1016/j.gr.2015.07.020.

Bodnar, R.J., 2003. Introduction to fluid inclusions. In: Samson, I., Anderson, A., Marshall, D. (Eds.), Introduction to Fluid Inclusions. Analysis and Interpretation Mineralogical Association of Canada, Fluid Inclusions, pp. 1–8.

Borojević Šoštarić, S., Cvetković, V., Neubauer, F., Palinkaš, L.A., Bernroider, M., Genser, J., 2012. Oligocene shoshonitic rocks of the Rogozna Mts. (Central Balkan Peninsula): Evidence of petrogenetic links to the formation of Pb–Zn–Ag ore deposits. Lithos 148, 176–195. https://doi.org/10.1016/j.lithos.2012.05.028.

Borojević Šoštarić, S., Palinkaš, A.L., Neubauer, F., Cvetković, V., Bernroider, M., Genser, J., 2014. The origin and age of the metamorphic sole from the Rogozna Mts., Western Vardar Belt: New evidence for the one-ocean model for the Balkan ophiolites. Lithos 192–195, 39–55. https://doi.org/10.1016/j.lithos.2014.01.011.

Boynton, W.V. 1984. Chapter 3 - Cosmochemistry of the Rare Earth Elements: Meteorite Studies. In: Henderson, P., editor. Developments in Geochemistry - Rare Earth Element Geochemistry. Elsevier. Vol. 2 p. 63-114. 10.1016/B978-0-444-42148-7.50008-3.

Cannell, J., Cooke, D.R., Walshe, J.L., Stein, H., 2005. Geology, mineralization, alteration, and structural evolution of the El teniente porphyry Cu-Mo deposit. Econ. Geol. 100 (5), 979–1003. https://doi.org/10.2113/gsecongeo.100.5.979.

Čifliganec, V., 1993. Copper mineralization in the republic of Macedonia: types and distribution patterns. Univ. Skopje Fac. Min. Geol.-Stip – Spec. Issue 1, 303.

Cooke, D.R., Hollings, P., Walshe, J.L., 2005. Giant porphyry deposits: characteristics, distribution, and tectonic controls. Econ. Geol. 100 (5), 801–818. https://doi.org/10.2113/gsecongeo.100.5.801.

Cooke, D.R., Hollings, P., Wilkinson, J.J., Tosdal, R.M. 2014. Geochemistry of Porphyry Deposits. In: Holland, H.D., Turekian, K.K., (Eds.). Treatise on Geochemistry, Second edition. Elsevier, Oxford. Vol. 13. p. 357-81. 10.1016/B978-0-08-095975-7.01116-5.

Cvetković, V., Prelević, D., Downes, H., Jovanović, M., Vaselli, O., Pécskay, Z., 2004. Origin and geodynamic significance of Tertiary postcollisional basaltic magmatism in Serbia (central Balkan Peninsula). Lithos 73 (3), 161–186. https://doi.org/10.1016/j.lithos.2003.12.004.

Das Sharma, S., Patil, D.J., Gopalan, K., 2002. Temperature dependence of oxygen isotope fractionation of CO2 from magnesite-phosphoric acid reaction. Geochim. Cosmochim. Acta 66 (4), 589–593. https://doi.org/10.1016/S0016-7037(01)00833-X.

Delibaş, O., Moritz, R., Selby, D., Göç, D., Revan, M.K., 2019. Multiple Porphyry Cu-Mo Events in the Eastern Pontides Metallogenic Belt, Turkey: From Early Cretaceous Subduction to Eocene Postcollision Evolution. Econ. Geol. 114 (7), 1285–1300. https://doi.org/10.5382/econgeo.4663.

Dilek, Y., Furnes, H., Shallo, M., 2007. Suprasubduction zone ophiolite formation along the periphery of Mesozoic Gondwana. Gondwana Res. 11 (4), 453–475. https://doi.org/10.1016/j.gr.2007.01.005.

Dimitrijević, M.D., 2001. Dinarides and the Vardar Zone: a short review of the geology. Acta Vulcanol. 13 (1–2), 1–8. https://doi.org/10.1400/19061.

Fontboté, L., Kouzmanov, K., Chiaradia, M., Pokrovski, G.S., 2017. Sulfide Minerals in Hydrothermal Deposits. Elements 13 (2), 97–103. https://doi.org/10.2113/gselements.13.2.97.

Fournier, R.O., 1999. Hydrothermal processes related to movement of fluid from plastic into brittle rock in the magmatic-epithermal environment. Econ. Geol. 94 (8), 1193–1211. https://doi.org/10.2113/gsecongeo.94.8.1193.

Goldstein, R.H., 2001. Fluid inclusions in sedimentary and diagenetic systems. Lithos 55 (1), 159–193. https://doi.org/10.1016/S0024-4937(00)00044-X.

Maps, G., 2020. Google Maps satellite image of the Vršnik open pit, Bučim mine, Northern Macedonia. Retrieved June 4, 2020, from. https://www.google.com/maps/@41.6682158,22.3556331,543m.

Grant, J.A., 2005. Isocon analysis: A brief review of the method and applications. Phys. Chem. Earth, Parts A/B/C 30 (17), 997–1004. https://doi.org/10.1016/j.pce.2004.11.003.

Harris, A.C., Golding, S.D., 2002. New evidence of magmatic-fluid–related phyllic alteration: Implications for the genesis of porphyry Cu deposits. Geology 30 (4), 335–338. https://doi.org/10.1130/0091-7613(2002)030<0335:neomfr>2.0.co;2.

Hastie, A.R., Kerr, A.C., Pearce, J.A., Mitchell, S.F., 2007. Classification of Altered Volcanic Island Arc Rocks using Immobile Trace Elements: Development of the Th–Co Discrimination Diagram. J. Petrol. 48 (12), 2341–2357. https://doi.org/10.1093/petrology/egm062.

Hoerler, J., Von Quadt, A., Burkhard, R., Peytcheva, I., Cvetkovic, V., Baker, T., 2022. The Karavansalija Mineralized Center (KMC) at the Rogozna Mountains in SW Serbia: Magma evolution and time relationship of intrusive events and skarn Au±Cu-Pb-Zn mineralization. Front. Earth Sci. 9, 1268. https://doi.org/10.3389/feart.2021.798701.

Irvine, T.N., Baragar, W.R.A., 1971. A Guide to the Chemical Classification of the Common Volcanic Rocks. Can. J. Earth Sci. 8 (5), 523–548. https://doi.org/10.1139/e71-055.

Johnson, J.W., Oelkers, E.H., Helgeson, H.C., 1992. SUPCRT92: A software package for calculating the standard molal thermodynamic properties of minerals, gases, aqueous species, and reactions from 1 to 5000 bar and 0 to 1000°C. Comput. Geosci. 18 (7), 899–947. https://doi.org/10.1016/0098-3004(92)90029-Q.

Karamata, S., 2006. The geological development of the Balkan Peninsula related to the approach, collision and compression of Gondwanan and Eurasian units. Geol. Soc., London, Spec. Publ. 260 (1), 155–178.

Klyukin, Y.I., Steele-Macinnis, M., Lecumberri-Sanchez, P., Bodnar, R.J., 2019. Fluid inclusion phase ratios, compositions and densities from ambient temperature to homogenization, based on PVTX properties of H2ONaCl. Earth Sci. Rev. 198, 102924 https://doi.org/10.1016/j.earscirev.2019.102924.

Kouzmanov, K., Pokrovski, G.S. 2012. Hydrothermal Controls on Metal Distribution in Porphyry Cu (-Mo-Au) Systems In: Hedenquist, J.W., Harris, M., Camus, F. (Eds.). Geology and Genesis of Major Copper Deposits and Districts of the World: A Tribute to Richard H Sillitoe. Society of Economic Geologists – Special Publication. Vol. 16. 10.5382/SP.16.

Kroll, T., Müller, D., Seifert, T., Herzig, P.M., Schneider, A., 2002. Petrology and geochemistry of the shoshonite-hosted Skouries porphyry Cu–Au deposit, Chalkidiki. Greece. Miner. Depos. 37 (1), 137–144. https://doi.org/10.1007/s00126-001-0235-6.

Le Bas, M.J., Le Maitre, R.W., Streckeisen, A., Zanettin, B., 1986. A Chemical Classification of Volcanic Rocks Based on the Total Alkali-Silica Diagram. J. Petrol. 27 (3), 745–750. https://doi.org/10.1093/petrology/27.3.745.

Lehmann, S., Barcikowski, J., Von Quadt, A., Gallhofer, D., Peytcheva, I., Heinrich, C.A., Serafimovski, T., 2013. Geochronology, geochemistry and isotope tracing of the Oligocene magmatism of the Buchim–Damjan–Borov Dol ore district: Implications for timing, duration and source of the magmatism. Lithos 180–181, 216–233. https://doi.org/10.1016/j.lithos.2013.09.002.

Lowell, J.D., Guilbert, J.M., 1970. Lateral and vertical alteration-mineralization zoning in porphyry ore deposits. Econ. Geol. 65 (4), 373–408. https://doi.org/10.2113/gsecongeo.65.4.373.

Márton, E., Toljić, M., Cvetkov, V., 2022. Late and post-collisional tectonic evolution of the Adria-Europe suture in the Vardar Zone. J. Geodyn. 149, 101880 https://doi.org/10.1016/j.jog.2021.101880.

Melfos, V., Voudouris, P., 2017. Cenozoic metallogeny of Greece and potential for precious, critical and rare metals exploration. Ore Geol. Rev. 89, 1030–1057. https://doi.org/10.1016/j.oregeorev.2017.05.029.

Melfos, V., Voudouris, P., Serafimovski, T., Tasev, G., 2019. Fluid Inclusions at the Plavica Au-Ag-Cu Telescoped Porphyry-Epithermal System, Former Yugoslavian Republic of Macedonia (FYROM). Geosciences. 9 (2), 88. https://doi.org/10.3390/geosciences9020088.

Molnár, K., Lahitte, P., Dibacto, S., Benkó, Z., Agostini, S., Döncző, B., Ionescu, A., Milevski, I., Szikszai, Z., Kertész, Z., Temovski, M., 2021. The westernmost Late Miocene-Pliocene volcanic activity in the Vardar zone (North Macedonia). Int. J. Earth Sci. 110 (8), 1–18. https://doi.org/10.1007/s00531-021-02153-2.

Moncada, D., Bodnar, R.J., 2012. Gangue mineral textures and fluid inclusion characteristics of the Santa Margarita Vein in the Guanajuato Mining District. Mexico. Centr. Eur. J. of Geosci. 4 (2), 300–309. https://doi.org/10.2478/s13533-011-0057-8.

Müller, D., Groves, D.I., 2016. Potassic Igneous Rocks and Associated Gold-Copper Mineralization, 4th Ed., Mineral Resource Reviews, Springer, 296 p. doi: 10.1007/978-3-319-23051-1_1.

Park, J.-W., Campbell, I.H., Malaviarachchi, S.P.K., Cocker, H., Hao, H., Kay, S.M., 2019. Chalcophile element fertility and the formation of porphyry Cu ± Au deposits. Miner. Depos. 54 (5), 657–670.

Peccerillo, A., Taylor, S.R., 1976. Geochemistry of eocene calc-alkaline volcanic rocks from the Kastamonu area. Northern Turkey. Contrib. to Mineral. Petrol. 58 (1), 63–81. https://doi.org/10.1007/BF00384745.

Perkins, R.J., Cooper, F.J., Condon, D.J., Tattitch, B., Naden, J., 2018. Post-collisional Cenozoic extension in the northern Aegean: The high-K to shoshonitic intrusive rocks of the Maronia Magmatic Corridor, northeastern Greece. Lithosphere. 10 (5), 582–601. https://doi.org/10.1130/l730.1.

Prelević, D., Foley, S.F., Romer, R.L., Cvetković, V., Downes, H., 2005. Tertiary Ultrapotassic Volcanism in Serbia: Constraints on Petrogenesis and Mantle Source Characteristics. J. Petrol. 46 (7), 1443–1487. https://doi.org/10.1093/petrology/egi022.

Radosavljević, S.A., Stojanović, J.N., Radosavljević-Mihajlović, A.S., Vuković, N.S., 2016. (Pb–Sb)-bearing sphalerite from the Čumavići polymetallic ore deposit, Podrinje Metallogenic District, East Bosnia and Herzegovina. Ore Geol. Rev. 72, 253–268. https://doi.org/10.1016/j.oregeorev.2015.07.008.

Richards, J.P., Boyce, A.J., Pringle, M.S., 2001. Geologic evolution of the Escondida area, northern Chile: A model for spatial and temporal localization of porphyry Cu mineralization. Econ. Geol. 96, 271–305. https://doi.org/10.2113/gsecongeo.96.2.271.

Révész, K.M., Landwehr, J.M., 2002. Delta13C and delta18O isotopic composition of $CaCO_3$ measured by continuous flow isotope ratio mass spectrometry: statistical evaluation and verification by application to Devils Hole core DH-11 calcite. Rapid Commun. Mass Spectrom.: RCM 16 (22), 2102–2114. https://doi.org/10.1002/rcm.833.

Reynolds, T.J., Beane, R.E., 1985. Evolution of hydrothermal fluid characteristics at the Santa Rita, New Mexico, porphyry copper deposit. Econ. Geol. 80 (5), 1328–1347. https://doi.org/10.2113/gsecongeo.80.5.1328.

Richards, J.P., 2003. Tectono-Magmatic Precursors for Porphyry Cu-(Mo-Au) Deposit Formation. Econ. Geol. 98 (8), 1515–1533. https://doi.org/10.2113/gsecongeo.98.8.1515.

Richards, J.P., 2009. Postsubduction porphyry Cu-Au and epithermal Au deposits: Products of remelting of subduction-modified lithosphere. Geology 37 (3), 247–250. https://doi.org/10.1130/g25451a.1.

Robertson, A.H.F., Trivić, B., Đerić, N., Bucur, I.I., 2013. Tectonic development of the Vardar ocean and its margins: Evidence from the Republic of Macedonia and Greek Macedonia. Tectonophysics 595–596, 25–54. https://doi.org/10.1016/j.tecto.2012.07.022.

Roedder, E. (Ed.), 1984. Fluid inclusions. De Gruyter.

Rosenbaum, J., Sheppard, S.M.F., 1986. An isotopic study of siderites, dolomites and ankerites at high temperatures. Geochim. Cosmochim. Acta 50 (6), 1147–1150. https://doi.org/10.1016/0016-7037(86)90396-0.

Rusk, B.G., Reed, M.H., Dilles, J.H., 2008. Fluid Inclusion Evidence for Magmatic-Hydrothermal Fluid Evolution in the Porphyry Copper-Molybdenum Deposit at Butte. Montana. Econ. Geol. 103 (2), 307–334. https://doi.org/10.2113/gsecongeo.103.2.307.

Serafimovski, T., Boev, B., 1996. Metallogeny of the Kratovo-Zletovo volcano-intrusive complex. Terranes of Serbia. 356, 347–352.

Serafimovski, T., Stefanova, V., Volkov, A.V., 2010. Dwarf copper-gold porphyry deposits of the Buchim-Damjan-Borov Dol ore district, Republic of Macedonia (FYROM). Geol. Ore. Depos. 52 (3), 179–195. https://doi.org/10.1134/S1075701510030013.

Serafimovski, T., Tasev, G., Strmić Palinkaš, S., Palinkaš, S.S., Gjorgijev, L., 2016. Porphyry Cu mineralizations related with the small Tertiary volcanic intrusions in the Bučim ore deposit. Geol. Croat. 69 (1), 101–119. https://doi.org/10.4154/GC.2016.09.

Seward, T.M., Williams-Jones, A.E., Migdisov, A.A. 2014. The chemistry of metal transport and deposition by ore-forming hydrothermal fluids. In: Holland, H.D., Turekian, K.K., (Eds.). Treatise on Geochemistry, Second edition. Elsevier, Oxford. Vol. 13. p. 29-57. 10.1016/B978-0-08-095975-7.01102-5.

Sharp, I.R., Robertson, A.H.F., 2006. Tectonic-sedimentary evolution of the western margin of the Mesozoic Vardar Ocean: evidence from the Pelagonian and Almopias zones, northern Greece. Geol. Soc. London Spec. Pub. 260 (1), 373–412. https://doi.org/10.1144/gsl.sp.2006.260.01.16.

Sillitoe, R.H., 2010. Porphyry Copper Systems. Econ. Geol. 105 (1), 3–41. https://doi.org/10.2113/gsecongeo.105.1.3.

Simpson, M.P., Strmić Palinkaš, S., Mauk, J.L., Bodnar, R.J., 2015. Fluid inclusion chemistry of adularia-sericite epithermal Au-Ag deposits of the southern Hauraki Goldfield. New Zealand. Econ. Geol. 110 (3), 763–786. https://doi.org/10.2113/econgeo.110.3.763.

Sinclair, W.D. 2007. Porphyry deposits. In: Goodfellow, W.D., editor. Mineral Deposits of Canada: A Synthesis of Major Deposit Types, District Metallogeny, the Evolution of Geological Provinces & Exploration Methods: Geological Association of Canada, Mineral Deposits Division – Special Publication nr. 5. p. 223-43. 10.2113/gsecongeo.102.7.1355.

Starkey, H.C., Blackmon, P.D., Hauff, P.L., 1984. The routine mineralogical analysis of clay-bearing samples. U.S.G.S. Bull. 1563, 1–32. https://doi.org/10.3133/b1563.
Steele-MacInnis, M., Bodnar, R.J., Naden, J., 2011. Numerical model to determine the composition of H2O–NaCl–CaCl2 fluid inclusions based on microthermometric and microanalytical data. Geochim. Cosmochim. Acta 75 (1), 21–40. https://doi.org/10.1016/j.gca.2010.10.002.
Steele-MacInnis, M., Lecumberri-Sanchez, P., Bodnar, R.J., 2012. HokieFlincs_H2O-NaCl: A Microsoft Excel spreadsheet for interpreting microthermometric data from fluid inclusions based on the PVTX properties of H2O–NaCl. Comput. Geosci. 49, 334–337. https://doi.org/10.1016/j.cageo.2012.01.022.
Stergiou, C.L., Melfos, V., Voudouris, P., Papadopoulou, L., Spry, P.G., Peytcheva, I., Dimitrova, D., Stefanova, E., Giouri, K., 2021. Rare and Critical Metals in Pyrite, Chalcopyrite, Magnetite, and Titanite from the Vathi Porphyry Cu-Au±Mo Deposit, Northern Greece. Minerals 11 (6), 630. https://doi.org/10.3390/min11060630.
Strmić Palinkaš, S., Palinkaš, L.A., Renac, C., Spangenberg, J.E., Lüders, V., Molnar, F., Maliqi, G., 2013. Metallogenic Model of the Trepča Pb-Zn-Ag Skarn Deposit, Kosovo: Evidence from Fluid Inclusions, Rare Earth Elements, and Stable Isotope Data. Econ. Geol. 108 (1), 135–162. https://doi.org/10.2113/econgeo.108.1.135.
Strmić Palinkaš, S., Wegner, R., Čobić, A., Palinkaš, L.A., De Brito Barreto, S., Váczi, T., Bermanec, V., 2014. The role of magmatic and hydrothermal processes in the evolution of Be-bearing pegmatites: Evidence from beryl and its breakdown products. Am. Mineral. 99 (2–3), 424–432. https://doi.org/10.2138/am.2014.4500.
Strmić Palinkaš, S., Palinkaš, L., Mandić, M., Roller-Lutz, Z., Pécskay, Z., Maliqi, G., Bermanec, V., 2016. Origin and K-Ar age of the phreatomagmatic breccia at the Trepca Pb-Zn-Ag skarn deposit, Kosovo: Implications for ore-forming processes. Geol. Croat. 69 (1), 121–142. https://doi.org/10.4154/GC.2016.10.
Strmić Palinkaš, S., Peltekovski, Z., Tasev, G., Serafimovski, T., Šmajgl, D., Rajič, K., Spangenberg, J.E., Neufeld, K., Palinkaš, L., 2018. The Role of Magmatic and Hydrothermal Fluids in the Formation of the Sasa Pb-Zn-Ag Skarn Deposit, Republic of Macedonia. Geosci. 8 (12), 444. https://doi.org/10.3390/geosciences8120444.
Strmić Palinkaš, S., Hofstra, A.H., Percival, T.J., Šoštarić, S.B., Palinkaš, L., Bermanec, V., Pecskay, Z., Boev, B., Muntean, J.L. 2018b. Comparison of the Allchar Au-As-Sb-Tl Deposit, Republic of Macedonia, with Carlin-Type Gold Deposits. In: Muntean, J.L., editor. Reviews in Economic Geology - Diversity in Carlin-Style Gold Deposits. Society of Economic Geologists. Vol. 20. 10.5382/rev.20.10.
Sun, W., Huang, R.F., Li, H., Hu, Y.B., Zhang, C.C., Sun, S.J., Zhang, L.P., Ding, X., Li, C. Y., Zartman, R.E., Ling, M.X., 2015. Porphyry deposits and oxidized magmas. Ore Geol. Rev. 65, 97–131. https://doi.org/10.1016/j.oregeorev.2014.09.004.
Sverjensky, D.A., Shock, E.L., Helgeson, H.C., 1997. Prediction of the thermodynamic properties of aqueous metal complexes to 1000°C and 5 kb. Geochim. Cosmochim. Acta 61 (7), 1359–1412. https://doi.org/10.1016/S0016-7037(97)00009-4.
Tasev, G., Serafimovski, T., 2012. Fluid inclusions study in the quartz from the Zletovo Mine. In: Geol. Macedonica Spec. Issue No 3, pp. 83–90. https://eprints.ugd.edu.mk/id/eprint/3139.
Taylor, H.P., 1997. Oxygen and hydrogen isotope relationships in hydrothermal mineral deposits. In: Barnes, H.L. (Ed.), Geochemistry of hydrothermal ore deposits, third edition. John Wiley, New York, pp. 229–302.
Taylor, H.P., Frechen, J., Degens, E.T., 1967. Oxygen and carbon isotope studies of carbonatites from the Laacher See District, west Germany and the Alno District. Sweden. Geochim. Cosmochim. Acta. 31, 407–430. https://doi.org/10.1016/0016-7037(67)90051-8.
Ulrich, T., Heinrich, C.A., 2002. Geology and Alteration Geochemistry of the Porphyry Cu-Au Deposit at Bajo de la Alumbrera. Argentina. Econ. Geol. 97 (8), 1865–1888. https://doi.org/10.2113/gsecongeo.97.8.1865.
Vanko, D.A., Bodnar, R.J., Sterner, S.M., 1988. Synthetic fluid inclusions: VIII. Vapor-saturated halite solubility in part of the system NaCl-CaCl2-H2O, with application to fluid inclusions from oceanic hydrothermal systems. Geochim. Cosmochim. Acta 52 (10), 2451–2456. https://doi.org/10.1016/0016-7037(88)90303-1.
Vasković, N.J., 2002. Petrology and P-T condition of white mica-chlorite schists from Vlasina series - Surdulica, SE Serbia. Ann. géol. de la Peninsule Balkanique 64, 199–220. https://doi.org/10.2298/GABP0264199V.
Velojić, M., Prelević, D., Jelenković, R., 2018. The origin of lead and sulphur in Tulare ore field, Lece magmatic complex, SE Serbia. Ann. géol. de la Peninsule Balkanique 79, 19–28. https://doi.org/10.2298/GABP1802019V.
Wang, R., Weinberg, R.F., Collins, W.J., Richards, J.P., Zhu, D.-C., 2018. Origin of postcollisional magmas and formation of porphyry Cu deposits in southern Tibet. Earth Sci. Rev. 181, 122–143.
Watanabe, Y., Sato, R., Sulaksono, A., 2018. Role of Potassic Alteration for Porphyry Cu Mineralization: Implication for the Absence of Porphyry Cu Deposits in Japan. Resour. Geol. 68 (2), 195–207. https://doi.org/10.1111/rge.12165.
Yanev, Y., Boev, B., Doglioni, C., Innocenti, F., Manetti, P., Pecskay, Z., Tonarini, S., D'Orazio, M., 2008. Late Miocene to Pleistocene potassic volcanism in the Republic of Macedonia. Mineral. Petrol. 94 (1-2), 45–60.
Zagorčev, I., Bončeva, I., 1988. Indications of Devonian basic volcanism in Southwest Bulgaria. Geol. Balcanica. 18 (4), 55–63.